toxins

MDPI

Article

Transcriptomic and Metabolomic Remodeling of the Cockroach Brain Following Envenomation by Parasitoid Wasp *Ampulex compressa*

Aleksei Miroliubov [1,2,*], Anastasia Lianguzova [2], Nadezhda A. Potapova [2,3], Albert Batushansky [4], Boris Efeykin [5] and Frederic Libersat [1]

1 Department of Life Sciences, Faculty of Natural Sciences, School of Brain Sciences and Cognition, Ben-Gurion University of the Negev, P.O. Box 653, Beer Sheva 8410501, Israel; libersat@bgu.ac.il
2 Laboratory of Host-Parasite Interactions, Zoological Institute, Russian Academy of Sciences, 1 Universitetskaya Embankment, Saint Petersburg 199034, Russia; anastasialianguzova@gmail.com (A.L.); nadezhdalpotapova@gmail.com (N.A.P.)
3 Association "Technological Platform BioTech 2030", 33 Leninsky Prospekt, Building 3, Moscow 119071, Russia
4 Ilse Katz Institute for Nanoscale Science and Technology, Ben-Gurion University of the Negev, P.O. Box 653, Beer Sheva 8410501, Israel; albertbat@bgu.ac.il
5 Center of Parasitology, A.N. Severtsov Institute of Ecology and Evolution, Russian Academy of Sciences, 33 Leninsky Prospekt, Moscow 119071, Russia; bocha19@yandex.ru
* Correspondence: miroliub@post.bgu.ac.il

Abstract

The parasitoid jewel wasp *Ampulex compressa* induces prolonged hypokinesia in its cockroach host, *Periplaneta americana*, by injecting venom into the central nervous system. Although acute behavioral effects are well characterized, molecular processes associated with persistent hypokinesia remain poorly understood. We combined transcriptomics and untargeted metabolomics to characterize brain changes 24 h after envenomation. RNA-seq of the central brain region containing the central complex and adjacent tissue identified 331 differentially expressed genes: 267 upregulated and 64 downregulated. Increased expression of *tyrosine decarboxylase-like* and arrestin-domain genes, together with reduced expression of a putative tyramine/octopamine receptor, suggests altered regulation of aminergic signaling. Changes in synaptic vesicle and innexin transcripts further implicate chemical and electrical synaptic function. Immune, detoxification, and extracellular-matrix genes were also affected. Independent metabolomic analyses revealed significant increases in fumaric acid and sorbitol, consistent with altered energy metabolism. Tyramine, octopamine, glutamate, and GABA showed no significant differences after multiple-testing correction, although several showed greater inter-individual variation in stung cockroaches. Together, these findings identify changes in neuromodulatory signaling, synaptic organization, and metabolic support as candidate processes associated with persistent hypokinesia. Their contributions to behavioral suppression remain to be distinguished from downstream responses to reduced neural activity and tissue stress.

Keywords: *Ampulex compressa*; *Periplaneta americana*; parasitoid wasp; behavioral manipulation; hypokinesia; transcriptomics; metabolomics; neuromodulation; central complex; host–parasite interactions

Check for updates

Received: 19 October 2026
Revised: 8 November 2026
Accepted: 13 November 2026
Published: 17 November 2026

Copyright: © 2026 by the authors. Licensee MDPI, Basel, Switzerland. This article is an open access article distributed under the terms and conditions of the Creative Commons Attribution (CC BY) license.

Key Contribution: At 24 h after *Ampulex compressa* envenomation, 331 differentially expressed genes implicate neural signaling, metabolism, and immunity. These transcriptional changes coexist with altered metabolite profiles and no FDR-significant differences in measured tyramine, octopamine, glutamate, or GABA, suggesting that persistent hypokinesia may involve changes in signaling regulation and metabolic support.

1. Introduction

Parasites that alter host behavior provide powerful model systems for investigating how one organism can modulate the physiology and neural activity of another. In some host–parasite associations, behavioural manipulation is mediated indirectly through systemic physiological changes, particularly when the parasite resides in the body cavity or internal organs, whereas in others the parasite localises within the host nervous tissue and, therefore, interacts directly with the nervous system [1–5]. However, even in well-studied systems, the molecular mechanisms responsible for the induction and long-term maintenance of manipulated behavior remain incompletely understood.

One of the most remarkable models of direct neural manipulation is the interaction between the parasitoid jewel wasp *Ampulex compressa* (Fabricius, 1781) and the American cockroach *Periplaneta americana* (Linnaeus, 1758). The adult female wasp is free-living, whereas its larva develops as a parasitoid on and subsequently inside the cockroach host. During an attack, the wasp delivers two precisely targeted stings. The first sting is directed into a thoracic ganglion and produces a brief paralysis of the front legs, lasting only a few minutes and facilitating the subsequent sting into the head ganglia [6,7]. Small venom molecules, including γ-aminobutyric acid (GABA), β-alanine, and taurine, contribute to this transient motor paralysis through their action on GABA receptors [8]. The second sting is delivered into the subesophageal and supraesophageal ganglia, injecting venom directly into the central nervous system and producing a markedly different and much more persistent behavioral effect.

Immediately after the head sting, the cockroach undergoes approximately 30 min of intense grooming, a phase driven primarily by venom-derived dopamine acting through D1-like receptors [9]. This is followed by a long-lasting hypokinetic state in which the cockroach retains the physical ability to walk but rarely initiates locomotion and displays reduced escape behavior and diminished responses to tactile, wind, and noxious stimuli [6,10]. Thus, the cockroach is not generally paralyzed; instead, the neural drive to initiate and maintain walking is selectively suppressed, while many other motor functions remain largely intact [11–13]. This behavioral state allows the wasp to lead the cockroach into a burrow, lay a single egg on it, and seal the entrance. The larva subsequently feeds on the living host before entering its body and completing development inside it [14]. Throughout much of this period, the cockroach remains alive but displays little effective defensive or escape behavior. Hypokinesia is reversible when subsequent parasitoid development is prevented. Arvidson et al. reported that the escape response returns to normal within 5–7 days if egg deposition is prevented [15].

Jewel-wasp venom contains a complex mixture of neuroactive compounds, peptides, and proteins capable of affecting membrane-associated targets as well as intracellular signaling pathways [15,16]. Previous transcriptomic analysis of the venom apparatus, combined with mass spectrometry-based proteomic analysis of collected venom, identified 264 venom proteins, providing a molecular inventory of candidate effectors [15]. A major neural target of the head sting is the central complex, a higher-order brain region involved in locomotor control, behavioral initiation, and sensorimotor integration. Focal injection of procaine,

a reversible blocker of voltage-dependent sodium channels, into the central complex is sufficient to produce a pronounced reduction in spontaneous walking [17]. Moreover, chronic electrophysiological recordings during venom infusion revealed a prolonged decrease in patterned central-complex activity, accompanied by reduced firing of descending interneurons projecting to thoracic locomotor circuits and decreased motor output [18]. These findings support a mechanistic sequence in which venom-induced suppression or reorganization of central-complex activity reduces descending locomotor drive, thereby initiating and maintaining hypokinesia. The reduced nocifensive responses of stung cockroaches further indicate that venom action affects not only locomotor initiation but also the neural processing of aversive or potentially damaging stimuli.

Previous HPLC-based comparisons of control and stung cockroaches found no depletion of dopamine, serotonin, octopamine, or tyramine in the central nervous system, arguing against monoamine depletion as the basis of venom-induced hypokinesia [19]. Although the behavioral and neurophysiological consequences of envenomation are increasingly well characterized, the molecular processes accompanying the prolonged manipulated state remain poorly understood. Because hypokinesia persists long after the acute behavioral effects of venom-derived neurotransmitters have subsided, envenomation may induce longer-lasting changes in host neural physiology, including alterations in gene expression, synaptic signaling, and metabolism. At the same time, direct penetration of the nervous system and venom injection are expected to trigger local injury, immune, detoxification, and tissue-repair responses. Distinguishing these overlapping components is therefore important for understanding the molecular state of the manipulated nervous system.

Here, we combined transcriptomic and untargeted metabolomic analyses to investigate the molecular changes associated with persistent venom-induced hypokinesia. We focused on the supraesophageal ganglion because it contains the central complex, a major target of the head sting and a brain region involved in the initiation and maintenance of locomotion. Previous behavioral and electrophysiological studies link venom-induced changes in this region to reduced descending locomotor drive, while stung cockroaches retain the capacity to execute coordinated movements [11–13,17,18]. This evidence motivated our focus on the molecular state of the brain, while recognizing that other ganglia may also contribute to behavioral suppression. Transcriptomic analysis targeted the central brain region containing the central complex and adjacent tissue, whereas untargeted metabolomics examined the supraesophageal ganglion excluding the optic lobes in an independent experiment. Both analyses were performed at 24 h after envenomation to characterize established hypokinesia after the initial grooming phase. We asked whether this state is associated with changes in neuromodulatory and synaptic pathways, how these relate to the measured neurotransmitter and metabolic profiles, and whether the molecular response also includes signatures of tissue stress, immunity, detoxification, and repair.

2. Results

2.1. Overview of the Transcriptional Response to Envenomation

Cockroaches exposed to the wasp were stung twice: first in the thoracic ganglia and then in the head, targeting the central complex and the subesophageal ganglion. Following the sting, cockroaches displayed approximately 30 min of intense grooming behavior while remaining in place. This phase was followed by a prolonged state of hypokinesia.

To investigate the molecular correlates of this behavioral manipulation, we generated bulk transcriptomic data from the central brain region adjacent to the central complex in two groups: untreated control cockroaches (C) and cockroaches sampled 24 h after wasp stinging (S). Samples are presented in Table 1.

Principal component analysis (PCA) showed separation between control and stung samples, primarily along PC1, which explained 47% of the total variance, while PC2 accounted for a further 19% (Figure 1). PERMANOVA confirmed significant multivariate differences between the two groups ($F = 7.85$, $R^2 = 0.50$, $p = 0.004$). Consistent with this separation, PC1 scores differed significantly between groups (ANOVA: $F = 12.05$, $p = 0.008$), whereas no significant difference was detected for PC2 ($p = 0.16$).

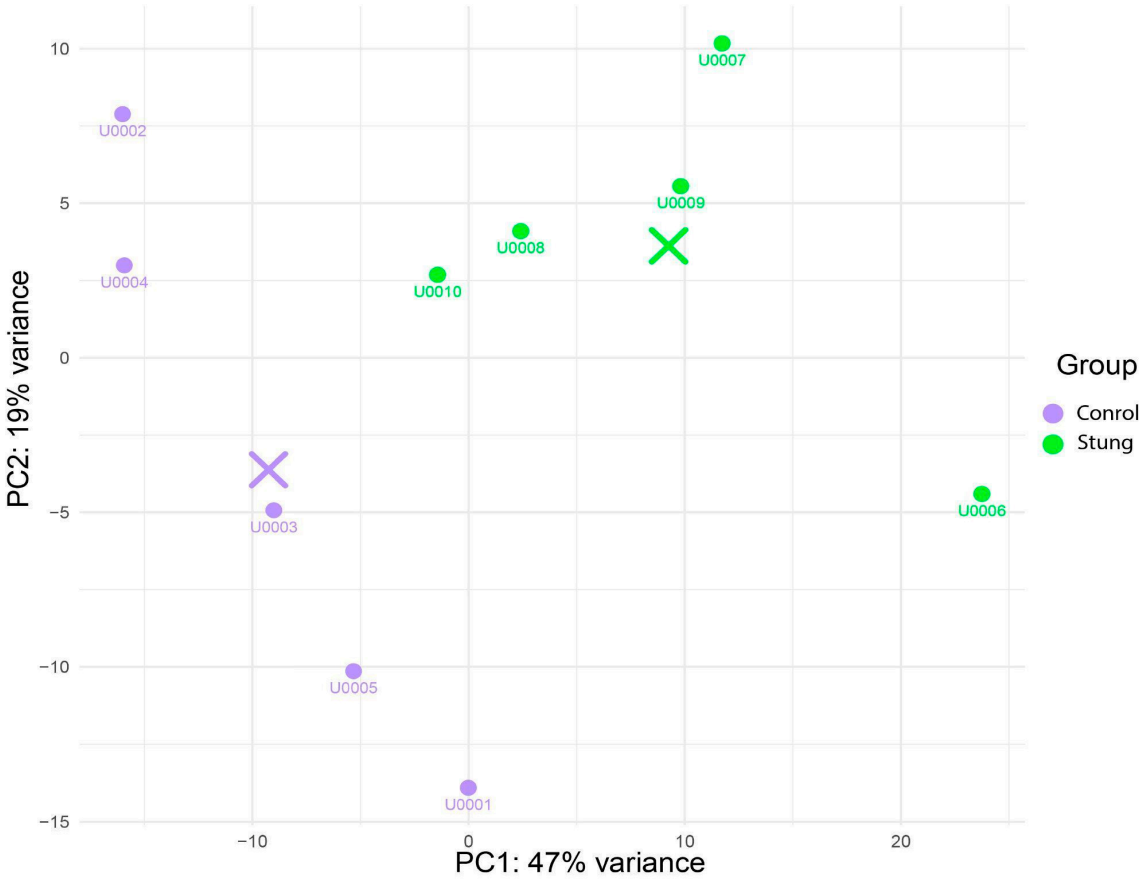


Figure 1. PCA of transcriptomic profiles from control and stung *Periplaneta americana*. Samples from control and *Ampulex compressa*-stung cockroaches are shown in purple and green, respectively. PC1 and PC2 explain 47% and 19% of the total variance. Crosses indicate group centroids.

Table 1. RNA-seq quality-control and alignment statistics for control and *Ampulex compressa*-stung *Periplaneta americana* samples. Each library represents pooled central brain tissue dissected from five adult male cockroaches. Stung animals were sampled 24 h after envenomation. Read counts indicate paired-end read pairs retained after trimming and quality filtering. Alignment rates are shown for the *P. americana* reference genome (PAMFEO1 priV1; GCF_040183065.1) and the OSA reference dataset. C, control; S, stung.

Sample Number	Sample Name	Control/Stung	Number of Read Pairs After QC and Trimming	Overall Alignment Rate to the *P. americana* Reference Genome	Overall Alignment Rate to OSA
1	CR446-001U0001	C	46,913,846	84.78%	0.11%
2	CR446-001U0002	C	40,701,391	84.93%	0.19%
3	CR446-001U0003	C	37,757,029	85.86%	0.14%
4	CR446-001U0004	C	58,838,637	87.14%	0.14%

Table 1. *Cont.*

Sample Number	Sample Name	Control/Stung	Number of Read Pairs After QC and Trimming	Overall Alignment Rate to the *P. americana* Reference Genome	Overall Alignment Rate to OSA
5	CR446-001U0005	C	38,522,634	85.33%	0.12%
6	CR446-001U0006	S	48,623,879	85.29%	0.15%
7	CR446-001U0007	S	51,386,863	87.60%	0.18%
8	CR446-001U0008	S	45,422,486	85.20%	0.13%
9	CR446-001U0009	S	40,968,378	90.42%	0.16%
10	CR446-001U0010	S	45,579,878	84.97%	0.14%

The volcano plot (Figure 2) illustrates the distribution of differentially expressed genes between the treatment and control groups. The *x*-axis shows the log2 fold change in gene expression, where positive values indicate genes upregulated in the treatment group and negative values indicate genes downregulated in the treatment group. The *y*-axis represents the statistical significance of differential expression as the −log10 adjusted *p*-value, with higher values indicating greater significance. Overall, the plot shows that the number of upregulated genes in the treatment group was substantially higher than the number of downregulated genes, with 267 upregulated and 64 downregulated genes passing the selected significance and fold-change thresholds. All differentially expressed genes are presented in Table S1. A subset of 60 genes selected for functional interpretation of the differences between control and stung central brain tissue is shown in Table 2.

Table 2. Selected differentially expressed genes in the central brain region containing the central complex and adjacent tissue of *P. americana* 24 h after stinging by *A. compressa*. Genes are grouped according to their putative functional roles in neuromodulation and neuronal signaling, as well as stress-, immune-, and injury-associated responses. Positive and negative log2FC values indicate higher and lower expression, respectively, in stung cockroaches relative to controls. Adjusted *p*-values are corrected for multiple testing. The check mark (✓) indicates genes associated with molecular functions that were also identified as significantly enriched in the GO enrichment analysis.

Gene ID/Symbol	Annotation	log2FC	Adjusted *p*-Value	GO Overlap
Neuromodulation and neuronal signaling				
Monoamine and catecholamine metabolism				
LOC138701054	aromatic-L-amino-acid decarboxylase-like (TDC)	1.29	0.0077	✓
LOC138711999	probable G-protein coupled receptor No18	−1.24	0.0064	
LOC138706378	arrestin domain-containing protein 17-like	1.39	0.0025	
LOC138706353	arrestin domain-containing protein 2-like	1.29	0.0013	
Inos	Inositol-3-phosphate synthase	−1.14	0.0127	
Pkc98E	Protein kinase C	−1.08	0.0124	
LOC138706194	multiple inositol polyphosphate phosphatase 1-like	1.81	0.0252	
LOC138691214	arylalkylamine N-acetyltransferase-like 2 (AANAT)	1.74	0.0107	
LOC138701862	protein yellow-like	1.28	0.0124	
Neuropeptide signaling and peptide turnover				
LOC138698787	adipokinetic hormone/corazonin-related peptide-like	−2.15	0.0138	
Nplp1	neuropeptide-like precursor 1	−1.02	0.0018	

Table 2. *Cont.*

Gene ID/Symbol	Annotation	log2FC	Adjusted *p*-Value	GO Overlap
LOC138695047	angiotensin-converting enzyme-like	2.08	0.0183	
LOC138716352	thyrotropin-releasing hormone-degrading ectoenzyme-like	1.54	0.0107	
Synaptic-vesicle release machinery				
LOC138712562	synaptic vesicle glycoprotein 2B-like	2.08	0.0119	
LOC138696606	protein unc-13 homolog 4B-like (Munc13)	1.52	0.0147	
LOC138701522	synaptic vesicle membrane protein VAT-1 homolog	1.21	0.0475	
Synapse remodeling				
LOC138694604	neural-cadherin	−1.38	0.0025	
LOC138694850	leucine-rich repeat neuronal protein 1-like	−1.38	0.0209	
Cals	calsyntenin 1	−1.14	0.0135	
LOC138698318	E3 ubiquitin-protein ligase Siah1-like	1.25	0.0074	
LOC138698288	E3 ubiquitin-protein ligase Siah1-like	1.99	0.0037	
LOC138715249	innexin inx3-like	3.15	0.0281	
LOC138715251	innexin inx3-like	2.39	0.0017	
LOC138715250	innexin inx3-like	2.27	0.0114	
LOC138713837	innexin shaking-B-like	2.37	0.0091	
Tollo	Toll-like receptor Tollo	1.98	0.0022	
Stress-, immune-, and injury-associated responses				
General neural activity and energy homeostasis				
Hr38	Hormone receptor-like in 38	−1.02	0.0125	
jus	julius seizure	−1.26	0.0043	
REPTOR	Repressed by TOR	1.44	0.0025	
LOC138705948	facilitated trehalose transporter Tret1-2 homolog	1.57	0.0304	
LOC138708841	facilitated trehalose transporter Tret1-like	1.44	0.0166	
LOC138705129	facilitated trehalose transporter Tret1-like	1.35	0.0167	
Innate immunity and the phenoloxidase cascade				
LOC138703264	phenoloxidase-activating factor 2	1.75	0.0024	
LOC138704540	phenoloxidase-activating factor 3-like	1.48	0.0076	
LOC138704536	CLIP domain-containing serine protease B4-like	1.39	0.0032	
LOC138703803	beta-1,3-glucan-binding protein-like	1.53	0.0033	
LOC138701110	beta-1,3-glucan-binding protein-like	3.18	0.0486	
LOC138713493	peptidoglycan-recognition protein SD-like	1.53	0.0243	
LOC138713503	peptidoglycan-recognition protein SC2-like	2.20	0.0051	✓
LOC138701518	lysozyme-like	2.83	0.0136	
LOC138694083	lysozyme c-1-like	2.03	0.0096	
LOC138701515	lysozyme-like	1.45	0.0383	
LOC138704148	termicin-like	2.17	0.0020	
Oxidative defence and venom detoxification				
LOC138712309	glutathione S-transferase 1-like	5.54	0.0034	
LOC138712317	glutathione S-transferase D5-like	3.49	0.0279	
LOC138690981	glutathione S-transferase 1-1-like	1.35	0.0050	
LOC138712138	cytochrome P450 4C1-like	2.59	0.0390	

Table 2. *Cont.*

Gene ID/Symbol	Annotation	log2FC	Adjusted *p*-Value	GO Overlap
LOC138712141	cytochrome P450 4C1-like	1.53	0.0034	
LOC138694679	cytochrome P450 4C1-like	1.18	0.0479	
LOC138698282	cytochrome P450 4C1-like	1.03	0.0115	
Tsf1	Transferrin 1	2.53	0.0275	
Extracellular-matrix remodeling and neural repair				
LOC138694616	matrilin-2-like	8.75	0.0021	
LOC138694611	cartilage matrix protein-like	1.66	0.0022	
LOC138709586	transforming growth factor-beta-induced protein ig-h3-like	2.47	0.0062	✓
LOC138709626	transforming growth factor-beta-induced protein ig-h3-like	1.38	0.0030	✓
LOC138713666	angiomotin-like	2.95	0.0099	
LOC138696403	putative fibroblast growth factor 1	1.17	0.0022	✓
LOC138710626	vascular endothelial growth factor A-A-like	2.14	0.0445	✓
Atf3	Activating transcription factor 3	1.45	0.0011	
LOC138702029	heat shock protein 70 A1-like	−1.45	0.0391	✓

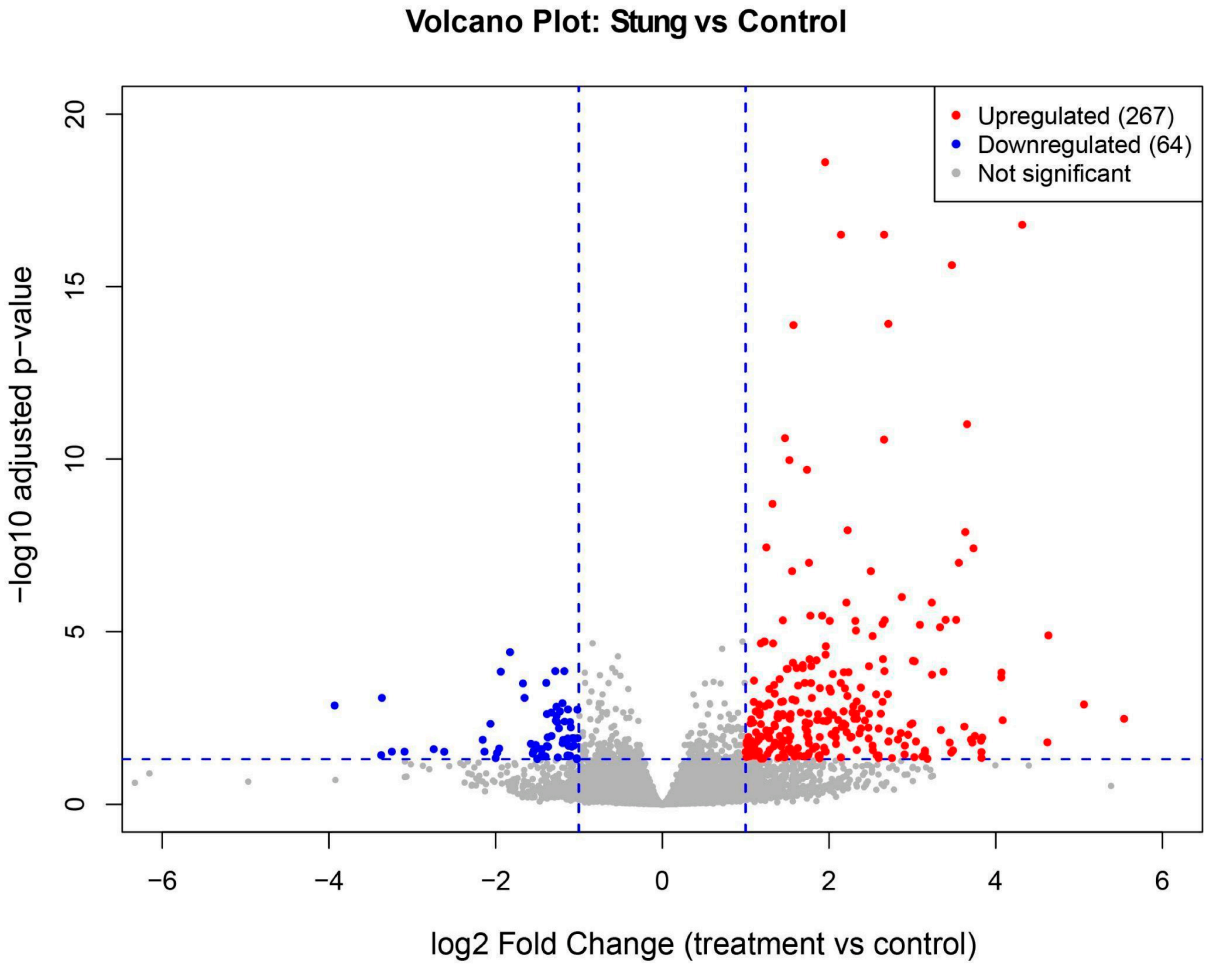


Figure 2. Volcano plot of differential gene expression between stung and control *P. americana*. The *x*-axis shows log2 fold change (stung vs. control), and the *y*-axis shows −log10 adjusted *p*-value. Red

points indicate significantly upregulated genes and blue points significantly downregulated genes, whereas grey points represent genes that did not meet the selected significance and fold-change criteria. Dashed lines indicate the applied thresholds ($|\log2FC| \geq 1$ and adjusted $p < 0.05$). In total, 267 genes were upregulated and 64 were downregulated in stung cockroaches relative to controls.

GO enrichment analysis identified several molecular functions that were significantly overrepresented among differentially expressed genes (Figure 3). Complete GO enrichment results for the Biological Process (BP), Molecular Function (MF), and Cellular Component (CC) categories are provided in Supplementary Tables S2–S7. The enriched molecular functions included lyase and oxidoreductase activities, extracellular matrix- and glycosaminoglycan-related binding functions, and several metabolic enzyme activities. Importantly, a subset of the enriched GO terms corresponded to functional changes independently identified in the differential expression analysis, including carboxy-lyase and carbon–carbon lyase activities, collagen binding, heparin binding, tyrosine decarboxylase activity, glycosaminoglycan binding, and extracellular matrix binding. These overlapping terms are highlighted by light-blue labels in Figure 3. Unfolded protein binding was the only function showing reduced representation.

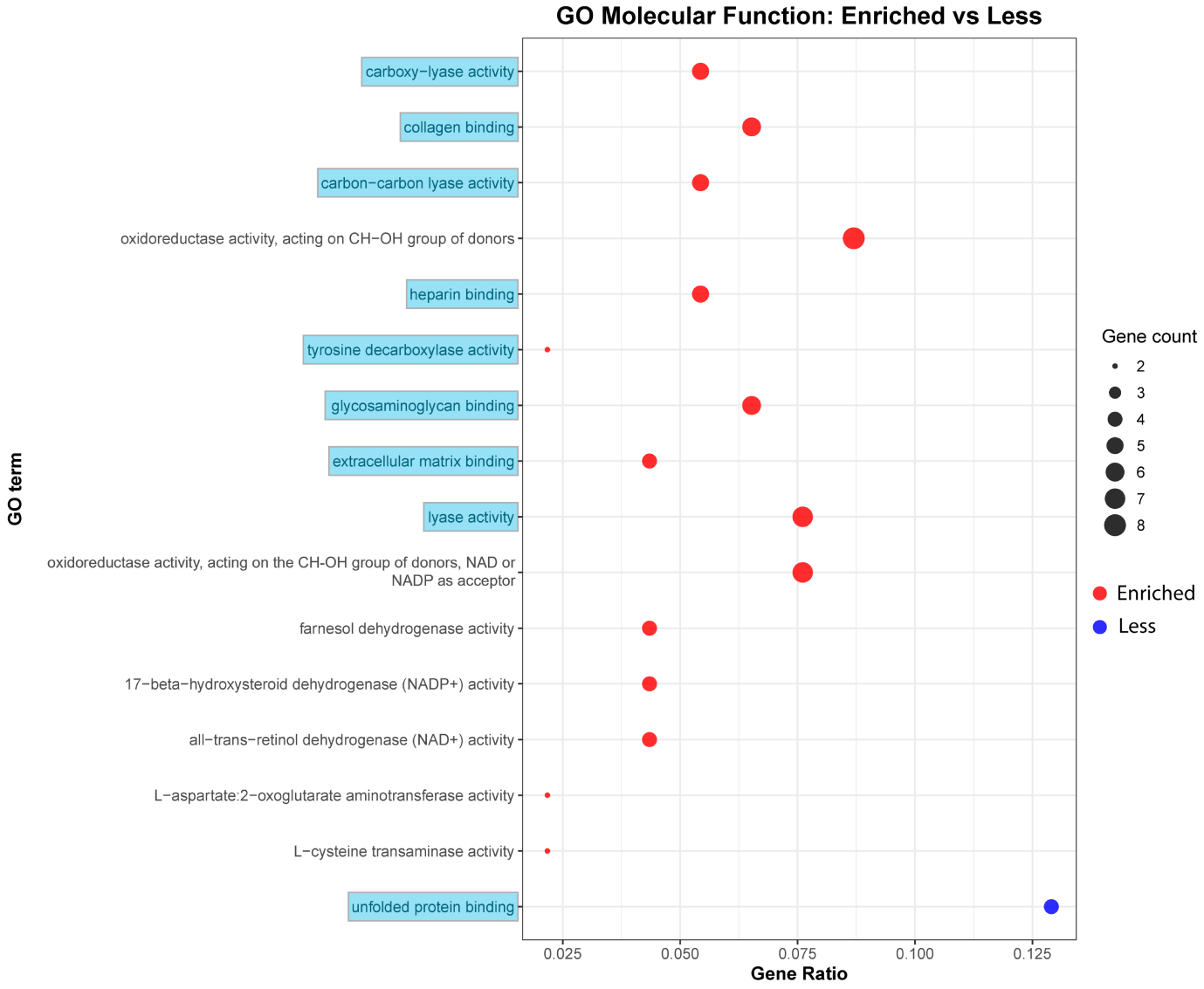


Figure 3. Gene Ontology (GO) Molecular Function enrichment analysis of differentially expressed genes. Enrichment analyses were performed separately for upregulated and downregulated gene

sets derived from RNA-seq data from five biological replicates per group. Each biological replicate consisted of pooled central brain tissue from five individual cockroaches. Red and blue indicate GO terms enriched among upregulated and downregulated genes, respectively. Dot size indicates the number of genes associated with each GO term, and the *x*-axis represents the gene ratio. GO terms highlighted with light-blue labels correspond to molecular functions also represented among the selected differentially expressed genes shown in Table 2.

2.2. Altered Pathways in the Stung Brain Region After Envenomation

Transcriptomic analysis of the central brain region containing the central complex and adjacent tissue revealed differential expression of genes associated with neuromodulation, neuropeptide signaling, synaptic transmission and remodeling, neuronal activity, energy homeostasis, innate immunity, detoxification, oxidative defence, and extracellular matrix organization.

To facilitate functional interpretation, we selected a subset of differentially expressed genes with the clearest putative relevance to the persistent behavioral phenotype and to the local response of nervous tissue to sting penetration and venom exposure (Table 2). These genes broadly separated into two overlapping functional groups. The first comprised genes associated with neural signaling, including monoamine and neuropeptide pathways, synaptic-vesicle machinery, electrical coupling, synaptic adhesion, and neuronal activity. The second comprised genes associated with tissue stress and injury responses, including innate immunity, phenoloxidase-related pathways, detoxification, oxidative defence, energy homeostasis, and extracellular matrix remodeling.

The complete set of significantly differentially expressed genes is provided in Table S1, whereas the selected functionally relevant genes and their expression changes are summarized in Table 2.

2.3. Metabolomic Changes Following Envenomation

Untargeted metabolomics was performed in both positive- and negative-ionization modes to compare control cockroaches with animals sampled 24 h after envenomation by *A. compressa*. PCA based on the relative abundance of detected features showed a trend toward separation of control and stung groups along the first principal component, accompanied by substantial within-group variability (Figure 4). In positive-ionization mode, PC1 and PC2 accounted for 36.5% and 17.1% of the total variance, respectively, whereas in negative-ionization mode they accounted for 40.2% and 16.1%. Within-group dispersion was particularly pronounced in the control group in both ionization modes.

In the positive-ionization dataset, 1142 metabolic features were detected, of which 334 received putative metabolite annotations and 34 were confirmed against the in-house library (Table S8). Statistical analysis identified 92 features that differed nominally between control and stung groups ($p < 0.05$), of which 27 remained significant after correction for multiple testing (FDR < 0.05). All 27 FDR-significant features showed higher abundance in the stung group, with log2 fold changes ranging from 0.26 to 1.64. However, none of these features corresponded to metabolites confirmed against the in-house library, and most lacked biologically interpretable metabolite annotations.

Among metabolites confirmed by the in-house library, cytosine and histidine showed nominal increases in the stung group, but neither passed FDR correction. Tyramine, octopamine, glutamate, and GABA showed no significant differences in relative abundance between groups after FDR correction. However, the stung group showed greater inter-individual dispersion for several of these metabolites, most notably tyramine and octopamine, despite the absence of a consistent shift in their central tendency. The distributions of these metabolites among individual control and stung cockroaches are shown in Figure 5.

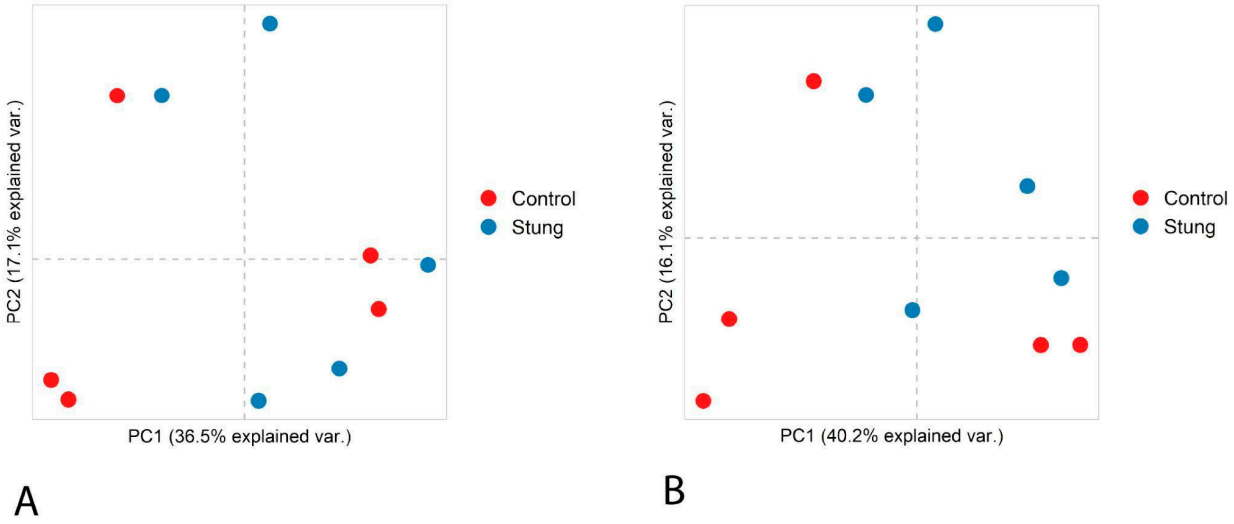


Figure 4. PCA of untargeted metabolomic profiles from control and envenomated cockroaches. PCA score plots based on relative metabolite-feature abundances: (**A**) positive-ionization mode, with PC1 and PC2 explaining 36.5% and 17.1% of total variance, respectively; (**B**) negative-ionization mode, with PC1 and PC2 explaining 40.2% and 16.1%, respectively. Control samples are shown in red and cockroaches sampled 24 h after *A. compressa* envenomation are shown in blue ($n = 5$ per group). The plots show a tendency toward separation between control and stung samples along PC1, accompanied by substantial within-group variability.

Several putatively annotated acylcarnitines showed nominal differences between groups. Propionylcarnitine, (R)-3-hydroxybutyrylcarnitine, C12-carnitine, and C14-carnitine showed higher abundance in stung cockroaches, whereas two features annotated as butenylcarnitine showed decreases. None of these features remained significant following FDR correction. Because their identities were not confirmed against authentic standards, these annotations were considered putative.

The negative-ionization dataset contained 1151 detected features, of which 325 received putative metabolite annotations (Table S9). Statistical analysis identified 234 features showing nominal differences between groups ($p < 0.05$), of which 18 remained significant after FDR correction. Seventeen of these features were increased in the stung group, whereas one was decreased (Table S9).

Among the FDR-significant negative-mode features, sorbitol was increased in stung cockroaches (log2FC = 0.75, approximately 1.68-fold; $p = 2.82 \times 10^{-4}$, FDR = 0.027), as was fumaric acid (log2FC = 0.26, approximately 1.20-fold; $p = 3.25 \times 10^{-4}$, FDR = 0.029). A further strongly increased feature was putatively annotated as oxalosuccinic acid (log2FC = 1.76, approximately 3.39-fold; $p = 2.11 \times 10^{-5}$, FDR = 0.012). Several other FDR-significant features remained unannotated or received database assignments that could not be confidently interpreted as endogenous cockroach metabolites.

Several additional metabolites showed nominal but not FDR-significant changes. Flavin mononucleotide increased in the stung group (log2FC = 0.42, $p = 0.0085$, FDR = 0.149), and two glutaric-acid features also showed nominal increases. Reduced glutathione did not differ significantly between groups.

Among the neurotransmitter-related metabolites analyzed in negative-ionization mode, GABA, glutamate, taurine, and aspartate showed no significant differences after correction for multiple testing. GABA showed a nominal increase (log2FC = 0.12, $p = 0.022$), but this difference did not remain significant after FDR correction (FDR = 0.200). Glutamate, taurine, and aspartate similarly showed no FDR-significant differences. Together with the positive-ionization data, these results indicate no FDR-significant differences in the relative

abundances of tyramine, octopamine, GABA, glutamate, taurine, or aspartate at 24 h. This conclusion is restricted to these reported analytes and does not establish unchanged levels of dopamine, serotonin, or other neurotransmitters.

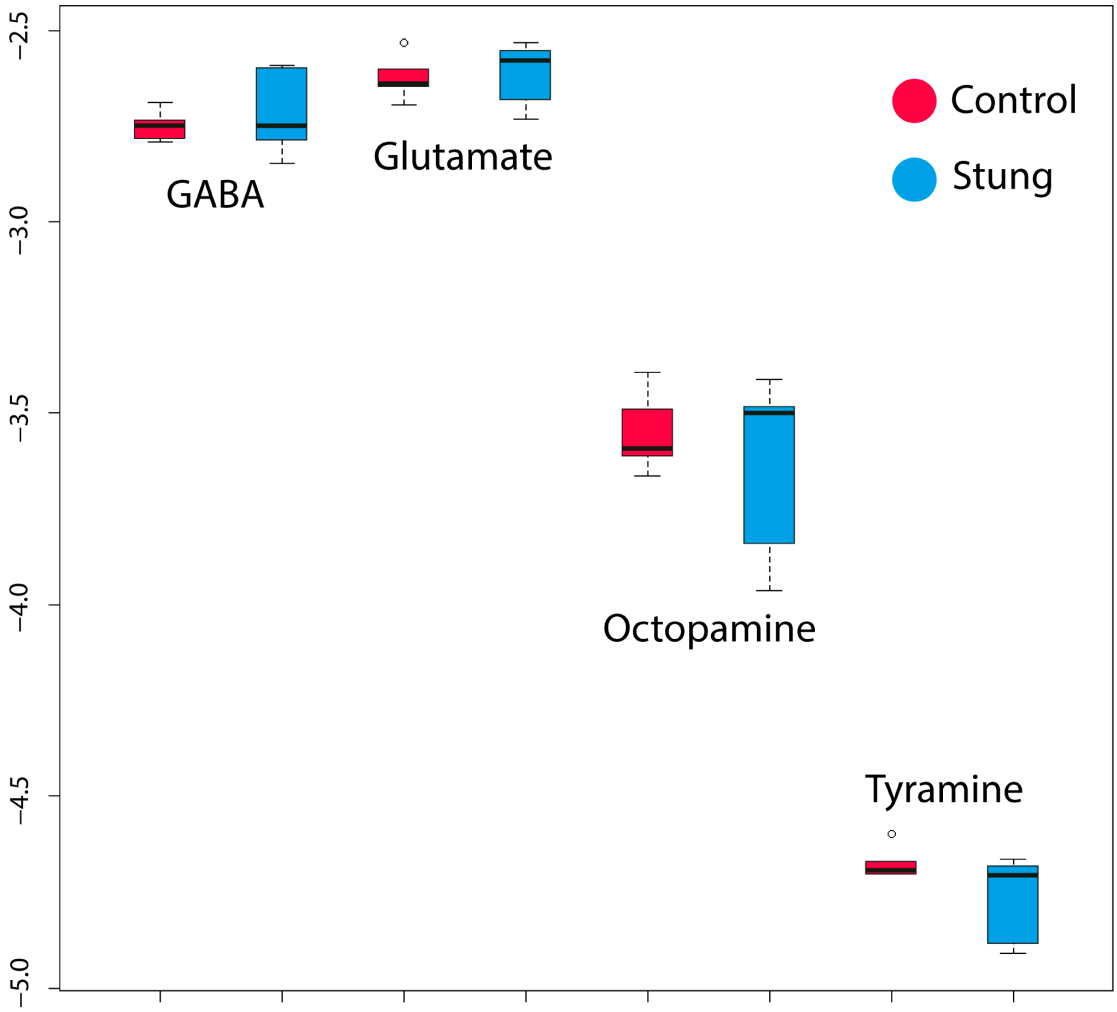


Figure 5. Relative abundance of selected neurotransmitters and neuromodulators in the cockroach brain 24 h after envenomation. Box plots show the normalized abundances of GABA, glutamic acid (glutamate), octopamine, and tyramine in the supraoesophageal ganglia of control cockroaches (red; $n = 5$) and cockroaches stung by *A. compressa* (blue; $n = 5$). Horizontal lines indicate medians, boxes represent the interquartile range, whiskers extend to 1.5 times the interquartile range, and open circles indicate outliers. None of the metabolites differed significantly between groups after FDR correction.

3. Discussion

3.1. Persistent Molecular Changes Following Envenomation

Envenomation by *A. compressa* produces a brief dopamine-dependent grooming phase followed by prolonged hypokinesia and reduced sensory responsiveness [6,9,10].

By 24 h after envenomation, the acute effects produced by venom-derived neurotransmitters such as dopamine and GABA are unlikely to depend on their continued extracellular presence, as these transmitters are subject to rapid transporter-mediated clearance and subsequent metabolic turnover in the insect nervous system [20–22]. Nevertheless, hypokinesia and reduced responsiveness persist. The transcriptional response observed at this time point therefore suggests that venom injection induces longer-lasting changes in molec-

ular pathways involved in arousal, sensory responsiveness, locomotor initiation, neural signaling, and tissue homeostasis.

In parallel, untargeted metabolomic profiling of the cockroach brain provided an independent view of the physiological state 24 h after envenomation. Importantly, the transcriptomic and metabolomic datasets were obtained from independent experiments and therefore should not be interpreted as direct sample-by-sample multi-omics correlations. Nevertheless, convergence between independently obtained molecular layers can identify pathways that are consistently affected by envenomation. To our knowledge, this represents the first untargeted metabolomic characterization of the cockroach nervous system following *A. compressa* envenomation.

Overall, the central brain region 24 h after stinging appears to be in a complex physiological state characterized by altered neuromodulation, reduced neuronal responsiveness, synaptic remodeling, metabolic adaptation, immune activation, detoxification, and extracellular matrix repair. Some of these responses may contribute directly to the persistent suppression of arousal and action initiation, whereas others are consistent with tissue stress, immune, and repair-associated responses whose contributions from mechanical injury, venom action, and secondary physiological changes cannot be distinguished here.

3.1.1. Monoamine and Catecholamine Metabolism

Tyramine and octopamine often exert opposing effects on locomotion and neuronal excitability, with octopamine generally promoting excitation and tyramine contributing to inhibitory modulation. Changes in their relative abundance can therefore tune locomotor activity according to the physiological state of the animal [23–25].

The upregulation of tyrosine decarboxylase (TDC) expression in the absence of a corresponding increase in tyramine β-hydroxylase (TBH) is notable because tyramine is produced from tyrosine by TDC and subsequently converted to octopamine by TBH. This transcriptional pattern could therefore alter the balance between tyramine and octopamine rather than simply increasing both pathways in parallel.

The metabolomic data provide an important complementary perspective. Despite the transcriptional changes in monoamine-related pathways, the mean abundance of tyramine and octopamine did not differ significantly between control and stung cockroaches after correction for multiple testing. GABA, glutamate, taurine, and aspartate also showed no FDR-significant differences in the reported metabolomic analyses. Previous targeted analyses likewise found no depletion of dopamine, serotonin, octopamine, or tyramine following *A. compressa* envenomation [19]. Together, these observations motivate investigation of changes in transmitter turnover and receptor regulation during persistent hypokinesia.

The combined data suggest altered regulation of neuromodulatory signaling despite the absence of FDR-significant differences in the reported transmitter abundances. Non-significant differences do not establish equivalence between groups and do not exclude changes in synthesis, release, degradation, receptor sensitivity, or local extracellular concentrations. Several neurotransmitters also showed marked inter-individual variation in the stung group, although the present sample size does not allow a robust conclusion that variance itself differs between experimental groups.

The downregulation of the putative tyramine/octopamine receptor may represent compensatory receptor desensitization in response to altered tyraminergic or octopaminergic signaling. Consistent with altered receptor regulation, two arrestin-domain-containing proteins were upregulated. Classical arrestins regulate G-protein-coupled receptor desensitization and internalization, while other arrestin-domain proteins participate in membrane-protein trafficking and turnover [26,27]. Borbor et al. found strongly reduced grooming after a second sting delivered 24 h after the first, and an attenuated response to a D1-like

dopamine receptor agonist at 6 h [28]. These behavioral findings motivate the hypothesis that altered receptor trafficking contributes to reduced dopaminergic responsiveness after envenomation. The functions and receptor targets of the cockroach arrestin-domain proteins require validation. Recovery of the agonist-induced response by one month also indicates that the persistent deficit in venom-induced grooming involves additional mechanisms [28].

A conceptual summary of the proposed tyraminergic changes is shown in Figure 6.

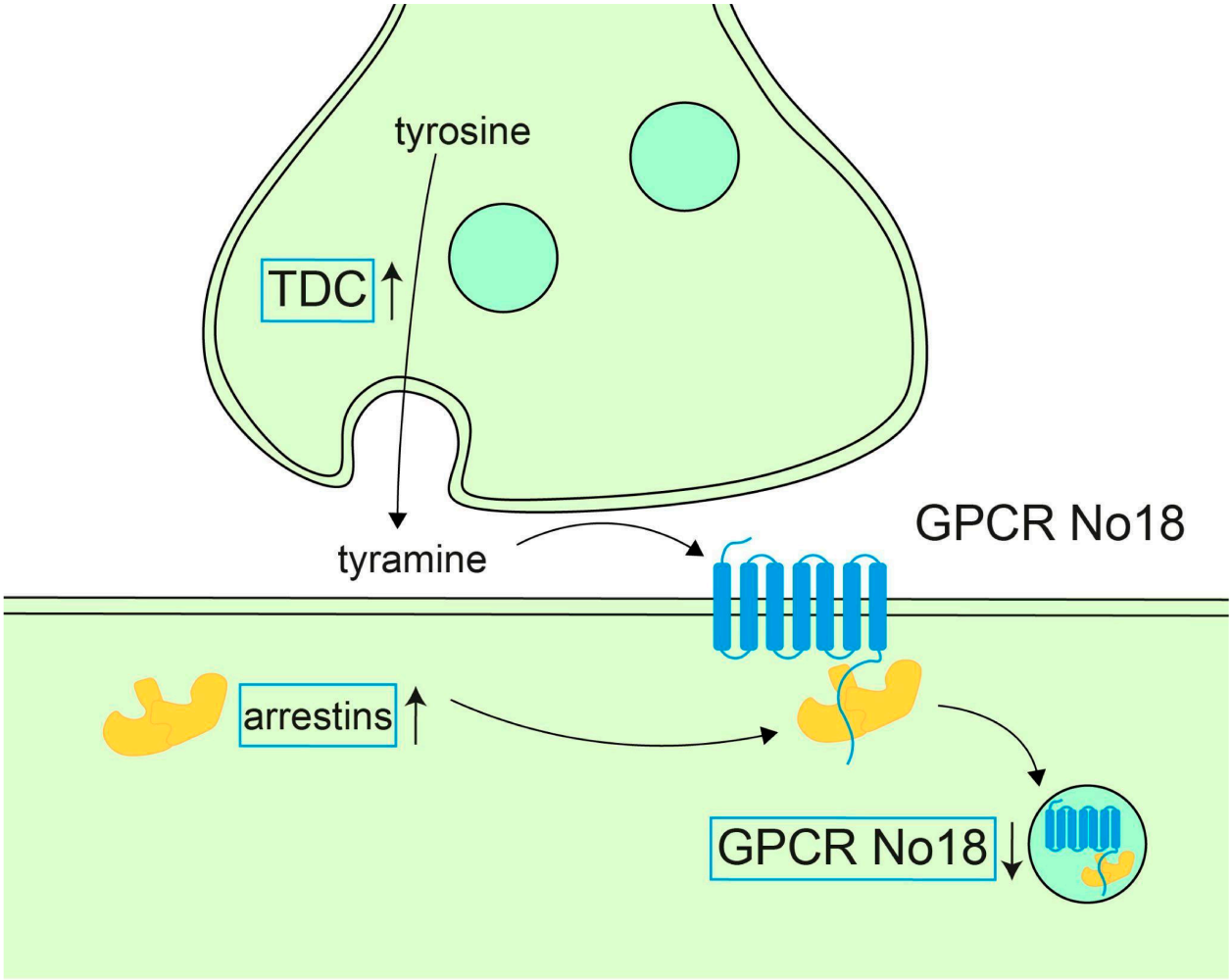


Figure 6. Proposed model of altered tyraminergic signaling in the cockroach brain 24 h after *A. compressa* envenomation. Upregulation of tyrosine decarboxylase-like (TDC-like) is consistent with altered tyramine synthesis, whereas downregulation of the putative tyramine/octopamine receptor GPCR No18, together with upregulation of arrestin-domain proteins, is consistent with enhanced receptor desensitization and/or internalization. Blue-highlighted components correspond to genes with differential transcript abundance. Upward and downward arrows beside these components indicate increased and decreased transcript abundance, respectively, in stung cockroaches relative to controls; they do not indicate measured changes in protein abundance or activity. Connecting arrows depict the proposed sequence of biochemical and signaling events. Receptor desensitization and internalization are hypothesized and were not directly measured.

Changes in phosphoinositide metabolism may further affect downstream sensory signaling. *Inos* downregulation could reduce de novo synthesis of myo-inositol and consequently decrease the availability of phosphatidylinositol and its phosphorylated derivatives, including phosphatidylinositol 4,5-bisphosphate (PIP_2) [29]. Reduced phosphoinositide

availability could affect downstream phospholipase C (PLC)-dependent signaling [30], although the relevant lipid intermediates and signaling activity were not measured.

Reduced diacylglycerol (DAG) availability could also affect DAG-dependent regulation of Munc13, a key component of synaptic vesicle priming. Consistent with reduced downstream phosphoinositide signaling, *Pkc98E* was also downregulated. In *Drosophila*, *Pkc98E* regulates sensory responses [31]. Reduced *Inos* and *Pkc98E* expression could therefore weaken phosphoinositide-dependent signal amplification downstream of receptor activation.

Conversely, *Mipp1-like* was upregulated, indicating broader remodeling of inositol-polyphosphate metabolism, although its products should not be directly equated with cytosolic PLC-generated inositol 1,4,5-trisphosphate (IP3) [32]. Together with the arrestin and receptor changes described above, these alterations may contribute to a state in which sensory information reaches the brain but is less effective in triggering downstream neuronal and motor responses.

The upregulation of arylalkylamine N-acetyltransferase-like 2 (AANAT) provides an additional mechanism by which aminergic signaling could be modified. Insect AANAT can acetylate dopamine, serotonin, tyramine, and octopamine and therefore represents an important route for monoamine inactivation [33,34]. Increased AANAT-like 2 expression could enhance monoamine turnover without necessarily altering their steady-state tissue abundance, providing a potential explanation for the coexistence of pronounced transcriptional changes and comparatively stable neurotransmitter concentrations.

Protein yellow-like was simultaneously upregulated, further supporting altered catecholamine-associated metabolism, although yellow-family proteins may also participate in melanization and wound-associated tissue remodeling [35,36].

3.1.2. Neuropeptide Signaling and Peptide Turnover

The downregulation of adipokinetic hormone/corazonin-related peptide-like (ACP) may be relevant to the persistent behavioral phenotype. ACP is expressed in discrete neurons and projections throughout the insect central nervous system and may function as a neurotransmitter or neuromodulator connecting anterior and posterior nervous-system regions [37,38]. Reduced ACP-like expression may consequently weaken central neuromodulatory communication and the metabolic support required for sustained locomotor activity.

Nplp1 was similarly downregulated. NPLP1-derived peptides are expressed in restricted neuronal populations and may participate in local neuromodulation, circadian regulation, and cellular stress protection [39,40]. Reduced *Nplp1* expression may therefore indicate both decreased peptidergic modulation and suppression of a stress-protective pathway.

At the same time, two potential neuropeptide-degrading peptidases were upregulated. Insect ACE-like peptidases may participate in neuropeptide processing and degradation within the nervous system [41,42].

Thyrotropin-releasing hormone-degrading ectoenzyme-like was also upregulated. Although its endogenous insect substrate is unknown, its annotation suggests a possible role in the metabolism of N-terminally pyroglutamylated peptides.

Together, reduced neuropeptide precursor expression and increased expression of potential peptide-degrading enzymes are consistent with a reduction in the duration or intensity of neuropeptide signaling. However, direct biochemical identification of the endogenous substrates of these enzymes will be required before their contribution to venom-induced behavioral manipulation can be established.

3.1.3. Synaptic-Vesicle Release Machinery

Synaptic vesicle glycoprotein 2B (SV2B) is a membrane protein associated with synaptic vesicles. The *SV2B-like* transcript increased approximately fourfold in stung cockroaches. In *Bombyx mori* (Linnaeus, 1758), disruption of synaptic vesicle glycoprotein 2B alters expression of genes involved in GABA synthesis, transport, and reception, suggesting an association with GABAergic transmission [43]. *SV2B-like* upregulation may therefore reflect remodeling of inhibitory signaling, although it does not directly demonstrate increased GABA release.

Protein unc-13 homolog 4B-like was also upregulated. UNC-13/Munc13 proteins are essential active-zone components that prime synaptic vesicles for fusion and link DAG-dependent neuromodulation to release probability [44,45]. The simultaneous upregulation of VAT-1-homolog provides additional evidence for altered vesicle-associated processes [46].

These changes may represent compensatory adjustment of neurotransmitter release in response to reduced receptor signaling or altered excitation–inhibition balance rather than a simple increase in synaptic activity.

A model of altered synaptic-vesicle release machinery is shown in Figure 7. Because several intermediate pathway components were not directly measured, this interpretation should be regarded only as a possible working model.

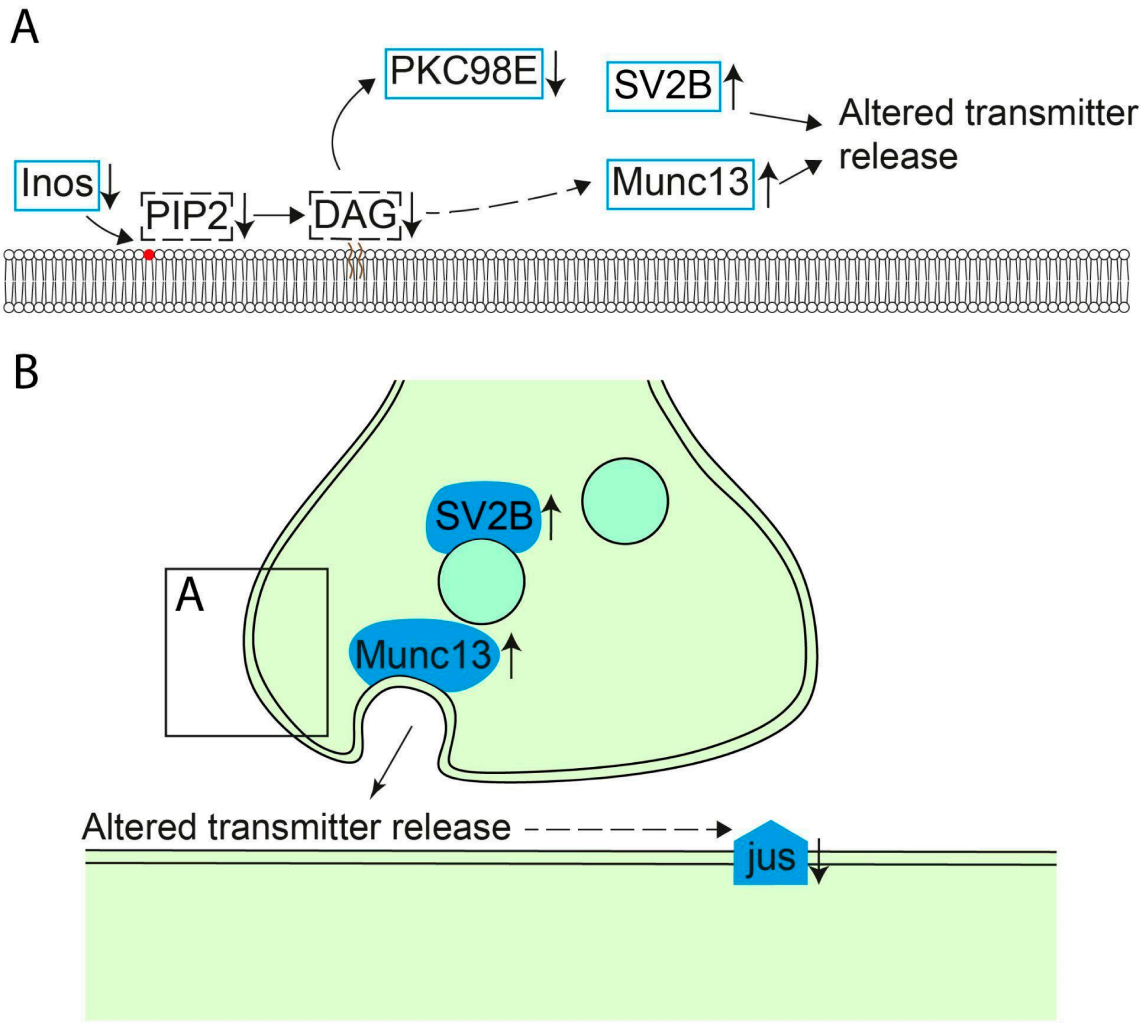


Figure 7. Proposed model of altered phosphoinositide signaling and synaptic release machinery 24 h after *A. compressa* envenomation. (**A**) Reduced *Inos* and *Pkc98E* expression may affect phosphatidylinositol 4,5-bisphosphate (PIP_2), diacylglycerol (DAG), and Munc13-dependent vesicle priming.

(**B**) Schematic synapse showing increased Munc13- and SV2B-like transcript abundance and decreased julius seizure-like (*jus*) transcript abundance in relation to proposed changes in synaptic output. The outlined region labeled A refers to panel A. Blue-highlighted components correspond to differentially expressed genes. Upward and downward arrows beside these components indicate increased and decreased transcript abundance, respectively; downward arrows beside PIP_2 and DAG indicate hypothesized, unmeasured decreases. Dashed boxes denote unmeasured intermediates, and dashed connecting arrows denote proposed functional links. Solid connecting arrows indicate pathway relationships or transmitter-release direction. Protein abundance, signaling activity, and transmitter release were not measured; this scheme represents a working model.

3.1.4. Synapse Remodeling

Synaptic remodeling may reflect both wound-repair mechanisms and venom-induced reorganization of neural circuits.

Downregulation of neural cadherin and leucine-rich repeat neuronal protein 1-like indicates possible changes in synaptic adhesion and circuit maintenance [47,48]. Reduced calsyntenin 1-like expression could also affect kinesin-dependent transport of receptors and other synaptic cargo; calsyntenins have been linked to neuronal receptor trafficking, learning, and behavioral responses to stress [49,50].

Upregulation of two *Siah1-like* transcripts may indicate increased stress-dependent ubiquitination and protein turnover.

In parallel, strong upregulation of three *inx3-like* transcripts and one *shaking-B-like* transcript suggests altered electrical coupling, circuit timing, or glia–neuron communication. Innexin Shaking-B is required for electrical transmission in the *Drosophila* giant-fibre escape pathway, whereas innexin 3 participates in electrical communication and tissue organization [51].

Importantly, increased innexin expression should not necessarily be interpreted as increased overall neuronal activity or simple synchronization. In *Drosophila*, the effects of electrical coupling on network synchrony depend on coupling strength [52].

Innexin upregulation in the stung cockroach central complex may therefore indicate reconfiguration of circuit timing, changing how neuronal ensembles synchronize or desynchronize their activity. Network synchrony can also promote quiescence and reduce sensory responsiveness in the *Drosophila* central complex [53], although its involvement in innexin-associated changes after envenomation remains untested.

Tollo/Toll-8-like upregulation may also contribute to this remodeling response. Beyond its immune role, Tollo can regulate synaptic growth through a non-canonical c-Jun N-terminal kinase-dependent pathway and neurotrophin-like Spätzle signaling [54].

Overall, this expression pattern is consistent with injury- or stress-associated remodeling of central-complex circuits and may disrupt the temporal coordination required for spontaneous locomotion and escape responses.

3.1.5. General Neural Activity and Energy Homeostasis

Hr38 is an insect orthologue of the nuclear receptor subfamily 4 group A family of immediate early genes. Its expression is induced by neuronal activation and correlates with stimulus-evoked behavior in insects; its downregulation therefore supports reduced activity-dependent transcription after stinging [18,55,56]. *Julius seizure* encodes a neuronal transmembrane protein whose disruption or knockdown causes seizure susceptibility in *Drosophila* [57], and it has also been examined in the context of motor-neuron molecular diversity [58]. Downregulation of the cockroach homolog therefore implicates a candidate regulator of excitability, although the direction of its effect on cockroach neural activity remains to be determined.

The transcriptional profile also indicates altered energy homeostasis. *REPTOR* was upregulated. REPTOR promotes stress resistance and maintenance of lipid and glycogen stores during nutrient limitation [59], making its increased expression compatible with a shift away from TORC1-supported anabolic activity towards metabolic conservation. However, REPTOR activity is primarily controlled by phosphorylation and nuclear localization, so transcriptional upregulation alone does not demonstrate TORC1 inhibition.

The coordinated upregulation of three *Tret1-like* transcripts may likewise represent a compensatory adaptation. In *Drosophila*, *Tret1-1* is expressed in perineurial glia and contributes to carbohydrate delivery to nervous tissue [60]. However, because the *Periplaneta* sequences appear more closely related to *Drosophila Tret1-2*, which did not transport trehalose in heterologous assays, their upregulation should be interpreted conservatively as evidence of altered sugar-transporter expression and carbohydrate handling rather than enhanced trehalose transport across glia [60].

The metabolomic dataset independently supports alteration of energy metabolism. Fumarate was significantly increased in stung cockroaches after correction for multiple testing. As an intermediate of the tricarboxylic acid cycle, altered fumarate abundance is consistent with modification of mitochondrial carbon metabolism. A second strongly increased feature was putatively annotated as oxalosuccinate, another TCA-associated metabolite, although its chemical identity requires confirmation.

Sorbitol was also significantly increased following envenomation. As a polyol linked to carbohydrate metabolism, its altered abundance may reflect changes in carbon utilization or intracellular carbohydrate handling. When considered together with *REPTOR* and *Tret1-like* upregulation, the independently obtained metabolomic and transcriptomic datasets therefore converge on altered energetic and carbohydrate metabolism.

Because both analyses used dissected tissue rather than isolated cell populations, the cellular origin of these metabolic responses remains unresolved.

Together with ACP-like downregulation and altered inositol metabolism, these transcriptomic and metabolomic changes suggest substantial redistribution of energy resources within the stung brain rather than simple global suppression of metabolism.

These metabolic changes may partly reflect altered neuronal energy demand following circuit suppression. Venom-induced reductions in central-complex activity and descending motor drive [18], together with *Hr38* downregulation in the present study, motivate this interpretation. Neural signaling has substantial ATP costs [61], so reduced activity could lower local energy demand and alter mitochondrial and carbohydrate metabolism. Increased fumarate and sorbitol abundance and *REPTOR* expression are compatible with metabolic adjustment, but do not establish reduced substrate turnover, ATP demand, or metabolic flux. Conversely, altered metabolic support, potentially involving ACP-like signaling [37,38], could contribute to maintaining hypokinesia. These possibilities are not mutually exclusive; distinguishing cause from consequence requires time-resolved measurements linking metabolism, neuronal activity, and behavior.

3.1.6. Innate Immunity and the Phenoloxidase Cascade

A component of the transcriptional response is consistent with tissue stress and injury-associated signaling following envenomation. The present design cannot separate effects of sting penetration, venom exposure, and secondary physiological changes.

The concurrent upregulation of prophenoloxidase-activating factor 2-like (PPAF2-like), prophenoloxidase-activating factor 3-like (PPAF3-like), and CLIP domain-containing serine protease B4-like (CLIPB4-like) is consistent with induction of components of the phenoloxidase protease cascade. In insects, PPAFs, also termed PPAEs or PAPs, are components of an

extracellular serine protease cascade that converts prophenoloxidase into active phenoloxidase, which oxidizes phenolic compounds and promotes melanin formation [62,63].

The CLIP family includes both catalytic proteases and non-catalytic cofactors of prophenoloxidase activation [64,65]. Because PPAF/CLIP nomenclature varies among insect species and does not reliably distinguish catalytic proteases from non-catalytic cofactors, the specific roles of the three *P. americana* transcripts cannot be inferred from annotation alone.

Their concurrent upregulation nevertheless supports coordinated activation of the phenoloxidase-associated response. Sterile local wounding alone can also activate a CLIP-domain protease/phenoloxidase cascade and induce a redox-dependent JNK-mediated cytoprotective response in neuronal tissue [66].

Because phenoloxidase-pathway components are predominantly associated with hemocytes and circulating hemolymph, their detection in central-complex tissue could reflect either local expression within neural tissue or infiltration or adhesion of hemocytes following injury. Notably, Kaiser et al. [16] also reported phenoloxidase upregulation in the central complex at the proteomic level. Together, these transcriptomic and proteomic observations support the possibility of a phenoloxidase-associated defence and repair response in the central complex rather than necessarily indicating microbial infection.

The upregulation of beta-1,3-glucan-binding protein-like transcripts and peptidoglycan-recognition proteins further supports activation of innate immune recognition pathways [67]. Beta-1,3-glucan-binding proteins may activate Toll- and phenoloxidase-associated protease cascades, whereas PGRP-SD-like likely reflects microbial or damage-associated recognition and Toll-pathway activation [68].

In contrast, PGRP-SC2-like is an amidase-type peptidoglycan-recognition protein capable of degrading peptidoglycan and limiting excessive IMD-pathway activation, suggesting that immune activation may be accompanied by negative-feedback or resolution mechanisms [69].

The induction of lysozyme transcripts, termicin-like, and transferrin 1 is consistent with activation of antimicrobial and antifungal defences, the prophenoloxidase/melanization response, iron sequestration, and protection against iron-mediated oxidative damage during injury-associated inflammation [70,71].

One possible interpretation is that the induction of pathogen-recognition and antimicrobial genes reflects a response to bacteria or fungi introduced into the nervous tissue during sting penetration. A second, more speculative possibility is that *A. compressa* venom actively promotes selected antimicrobial and antifungal responses in the host, helping to preserve the hypokinetic cockroach as a viable food source for the developing larva.

Other parasitoid systems provide an indirect precedent: *Cotesia vestalis* teratocytes express antimicrobial factors that can improve host survival after pathogen challenge [72]. Testing a host-preservation function for *A. compressa* venom will require experiments linking venom exposure and induced immune responses to microbial resistance and host survival.

In addition, antimicrobial peptides are known components of solitary wasp venoms and may help prevent infection after prey envenomation [73]. However, this interpretation should remain cautious because parasitoid venoms can also suppress host immune pathways, including prophenoloxidase activation and antimicrobial peptide synthesis, to protect parasitoid eggs or larvae from host immune attack [74].

Thus, in the *A. compressa–P. americana* system, immune-gene upregulation may represent a combination of mechanical injury, possible microbial contamination, and potentially host-preservation responses induced or facilitated by the wasp.

3.1.7. Oxidative Defence and Venom Detoxification

The strongest detoxification response involved glutathione S-transferases (GST). GSTs conjugate electrophilic xenobiotics with glutathione and protect cells from lipid-peroxidation products and oxidative damage [75–78]. Their coordinated induction therefore indicates substantial activation of redox- and detoxification-related pathways in the stung central brain region.

The metabolomic results provide a useful constraint on this interpretation. Despite strong GST upregulation, reduced glutathione itself remained comparatively stable. Thus, the transcriptional response may reflect activation of mechanisms maintaining redox homeostasis rather than severe depletion of the glutathione pool. Consequently, the transcriptomic data currently provide stronger evidence for activation of detoxification and oxidative-defence pathways than the metabolomic dataset.

The upregulation of four *CYP4C1-like* transcripts suggests additional activation of local cytochrome P450-dependent metabolism. Although insect cytochrome P450-mediated detoxification is commonly associated with the fat body and Malpighian tubules, brain-enriched cytochrome P450 enzymes can protect nervous tissue directly from neuroactive xenobiotics [79]. Cytochrome P450 family 4 enzymes may also metabolize fatty acids and injury-associated lipid mediators [80].

The strong increase in transferrin 1 provides another potentially protective mechanism. By binding free iron released from damaged cells, transferrin can restrict iron-dependent production of reactive oxygen species and may also contribute to antimicrobial defence [81–84].

Collectively, GST, cytochrome P450, and transferrin induction indicates a coordinated protective response against venom components, oxidative stress, and secondary cellular damage.

3.1.8. Extracellular-Matrix Remodeling and Neural Repair

In insects, the nervous system is closely associated with extracellular-matrix structures, including the neural lamella, and glia–ECM interactions are required for nervous-system organization and remodeling [85].

The strong induction of matrilin-family transcripts suggests substantial ECM network reorganization after envenomation. Matrilin-2-like was the most strongly upregulated transcript in the selected dataset, and cartilage matrix protein-like was also increased.

Matrilins organize extracellular-matrix networks [86,87] and have been associated with neural repair in vertebrates [88,89], providing a comparative basis for investigating the functions of the cockroach homologues.

Thus, coordinated upregulation of matrilin-2-like and cartilage matrix protein-like may support structural stabilization, glial-like repair responses, and regeneration-associated remodeling around damaged neural tissue.

The two upregulated *TGFBI/βig-h3-like* transcripts provide additional evidence for such a response. TGFBI is associated with cell–matrix adhesion and injury responses in vertebrates [90,91], but the cellular source and function of the cockroach *TGFBI-like* transcripts remain unresolved.

Angiomotin-like and *FGF1-like* induction may indicate changes in cell migration and tissue remodeling, based on functions described for related proteins [92–97].

ATF3 upregulation provides additional support for an injury-related response. ATF3 is a stress-inducible transcription factor strongly associated with neuronal injury, axonal regeneration, and pro-regenerative transcriptional programmes [98,99].

HSP70 A1-like was downregulated at 24 h post-sting, indicating a heterogeneous transcriptional stress response alongside the induced repair-associated genes [100]. Establishing whether these signatures accompany neuronal survival or cell loss requires direct

histological and cell-death measurements. The reported recovery of escape behavior after envenomation [15] supports a reversible component of venom action, while the extent of local structural injury remains unresolved.

Together, these expression changes are consistent with extracellular-matrix remodeling and injury-associated repair signaling in the sampled central brain region 24 h after envenomation.

Although this ECM signature is probably not a direct mechanism of behavioral manipulation, it may influence central-complex function indirectly by changing the extracellular environment, tissue stability, and neuron–glia interactions during the prolonged hypokinetic state.

3.2. Temporal Interpretation and Limitations

The 24 h time point was selected to characterize the established hypokinetic state after the initial grooming phase, rather than the immediate pharmacological effects of venom. Transcript abundance and metabolite concentrations need not respond with the same temporal dynamics, and time-lagged relationships between these molecular layers have been demonstrated in other systems [101–104]. Earlier transient changes in neurotransmitter concentrations could therefore have subsided before sampling, whereas other metabolic responses might emerge later. A single time point cannot distinguish these possibilities or establish whether the observed changes initiate, maintain, or follow behavioral suppression. Time-course sampling spanning the acute response, established hypokinesia, and subsequent recovery would help distinguish transient from persistent responses and test their temporal relationship to behavior. Targeted reverse-transcription quantitative PCR (RT-qPCR) across these time points could validate the expression trajectories of candidates such as TDC-like, arrestin-domain genes, *Hr38*, and *REPTOR*. Combining these measurements with behavioral assays, targeted metabolite quantification, and electrophysiological recordings would help relate molecular changes to neural activity and recovery.

The independent experiments and different sampling designs also limit integration: the transcriptomic analysis targeted the central brain region containing the central complex and adjacent tissue, whereas metabolomics used the supraesophageal ganglion excluding the optic lobes. Transcriptomic replicates pooled tissue from five cockroaches, whereas metabolomic replicates represented single individuals. Agreement between these datasets therefore supports pathway-level hypotheses rather than direct transcript–metabolite or cell-specific relationships.

The anatomical scope of the study also limits interpretation. Neither the subesophageal ganglion nor the thoracic ganglia were profiled, although both are relevant to the control of locomotion. Comparing these ganglia with the supraesophageal brain would help distinguish local molecular responses from changes distributed across descending and segmental motor pathways.

Finally, differential transcript abundance does not establish changes in protein activity, synaptic function, or causality. Functional assignments based on sequence annotation require validation, and the immune- and repair-associated signatures do not demonstrate the extent of structural damage or distinguish mechanical injury from venom-specific effects. Histological analysis, appropriate injury controls, and functional perturbation of candidate pathways will be needed to resolve these alternatives.

4. Conclusions

The *Ampulex compressa–Periplaneta americana* host-parasitoid system provides a model for investigating persistent yet reversible behavioral manipulation. Recovery of escape responses when parasitoid development is prevented [15] makes this system particularly

suitable for studying the molecular processes associated with behavioral suppression and subsequent recovery. Here, we characterize the host brain transcriptional response together with, to our knowledge, the first untargeted metabolomic analysis of the cockroach nervous system following *A. compressa* envenomatio.

At 24 h after envenomation, the cockroach nervous system showed extensive transcriptional reorganization affecting monoamine and neuropeptide signaling, synaptic-vesicle machinery, electrical and chemical synaptic organization, neuronal activity, energy homeostasis, innate immunity, detoxification, and extracellular-matrix repair. These responses appear to comprise overlapping components: alterations in neuromodulatory and synaptic pathways that may contribute to persistent hypokinesia, and injury-, immune-, detoxification-, and repair-associated responses potentially associated with venom exposure, sting penetration, or secondary physiological changes.

The metabolomic data provide an independent and complementary view of this prolonged physiological state. Despite pronounced transcriptional changes in neuromodulatory pathways, tyramine, octopamine, GABA, glutamate, taurine, and aspartate showed no FDR-significant differences in the reported metabolomic analyses. These results provide no evidence of depletion of these compounds at 24 h, but do not establish unchanged levels of all neurotransmitters. Instead, changes in neurotransmitter turnover, receptor signaling, vesicle release, electrical coupling, and synaptic organization may alter neural circuit function without substantially changing bulk transmitter concentrations.

The metabolomic analysis also revealed FDR-significant changes consistent with altered energy metabolism, including increased fumarate and sorbitol. Together with the independent transcriptional upregulation of *REPTOR* and *Tret1-like* transporters, these findings indicate that envenomation is accompanied by changes in mitochondrial and carbohydrate metabolism. Because the transcriptomic and metabolomic datasets were obtained from independent experiments, this convergence should be interpreted at the pathway level rather than as direct correspondence between individual transcripts and metabolites.

Taken together, our results support a model in which *A. compressa* envenomation induces a prolonged reorganization of host neural physiology rather than simply suppressing neural activity through depletion of signaling molecules. Persistent hypokinesia may arise from coordinated changes in neuromodulatory signaling, synaptic and circuit organization, and metabolic support, accompanied by transcriptional signatures consistent with tissue stress and repair, whose relationship to structural injury remains unresolved. Applying the previously established proteomics pipeline to central brain tissue collected under matched experimental conditions would test whether transcriptional changes are accompanied by corresponding protein-level alterations [16]. Time-resolved transcriptomic, proteomic, and targeted metabolomic analyses will be important for distinguishing temporary from persistent responses and for identifying the venom-derived factors and host pathways responsible for establishing and maintaining this remarkable behavioral state.

5. Materials and Methods

5.1. Cockroach Rearing and Experimental Animals

Ampulex compressa (Hymenoptera: Ampulicidae) wasps and *P. americana* cockroaches were maintained in crowded laboratory colonies under controlled conditions (30 °C, 40–60% relative humidity, 12 h light:12 h dark photoperiod). Water and food were provided ad libitum; cockroaches were fed cat chow, and wasps were supplied with honey. To obtain stung cockroaches, individual male cockroaches were introduced to a single wasp and allowed to be stung. Control and stung cockroaches were maintained under identical conditions, differing only in exposure to the wasp. The experiments performed comply

with Principles of Animal Care, NIH publication no. 86-23, revised in 1985, and also with the current laws of the State of Israel.

5.2. Transcriptomic Research Experimental Design and RNA Sequencing

Two experimental groups were used: a control group (C), consisting of adult male cockroaches, and a stung group (S), consisting of adult male cockroaches sampled 24 h after stinging by the parasitoid wasp. We selected 24 h after envenomation to examine an established hypokinetic state characterized by reduced spontaneous locomotion and behavioral responsiveness [105]. Sampling at this stage allowed us to investigate molecular changes associated with the sustained behavioral effects of venom after the initial grooming phase and transient thoracic paralysis [8,9,12]. We used only adult males to avoid any disturbances from the reproductive cycle in females. Each biological replicate represented a pooled sample of five dissected brain regions adjacent to the central complex. In total, five biological replicates were prepared for each group (Figure 8).

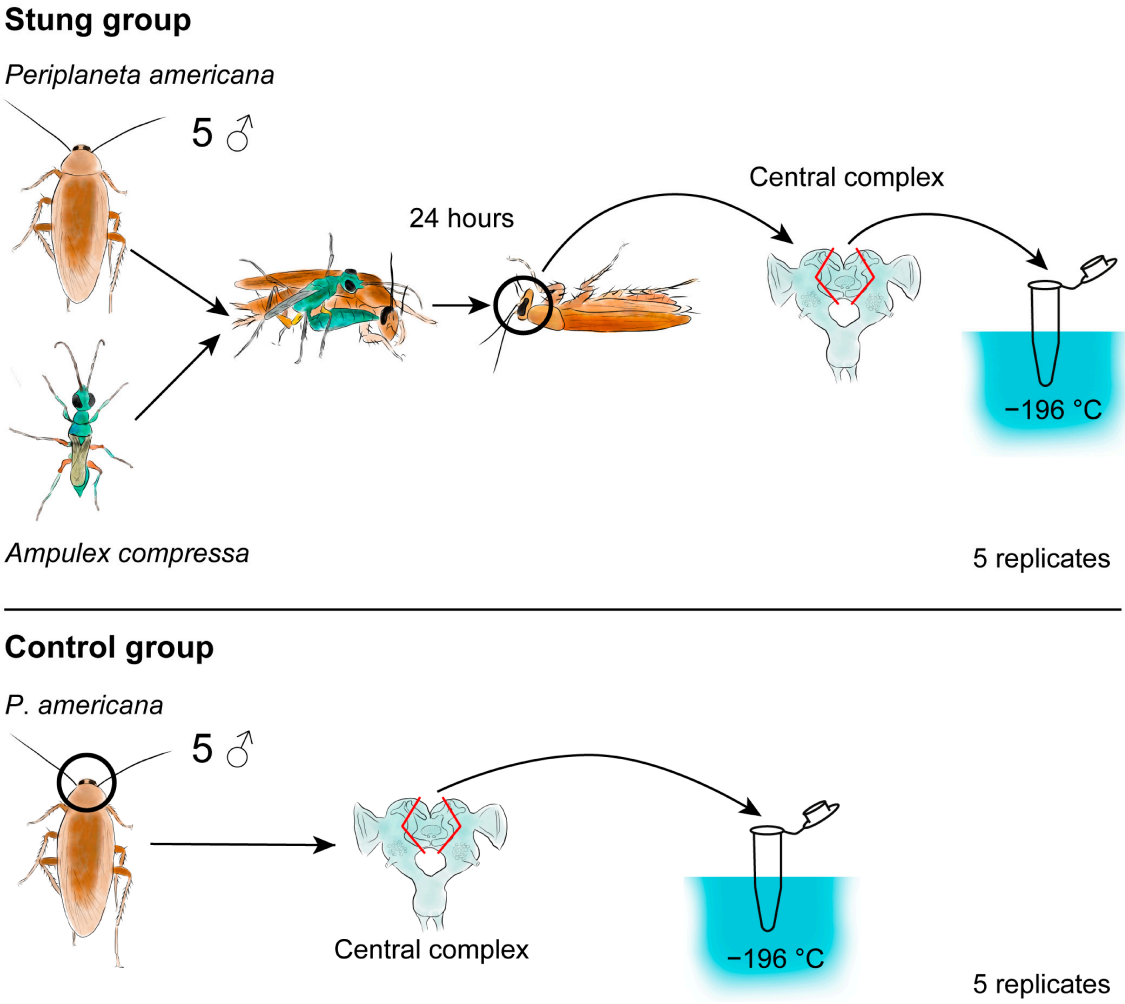


Figure 8. Experimental design and tissue sampling for transcriptomic analysis. Adult male *Periplaneta americana* were assigned to control and stung groups. Cockroaches in the stung group were exposed to *Ampulex compressa* and sampled 24 h after stinging, while control animals were maintained under identical conditions without exposure to the wasp. The central region of the supraesophageal ganglion containing tissue adjacent to the central complex was dissected and immediately snap-frozen in liquid nitrogen. Each biological replicate consisted of pooled tissue from five cockroaches, and five biological replicates were prepared per group (n = 25 cockroaches per group).

To minimize possible circadian effects on gene expression, all dissections were performed at approximately the same time of day (around 11:00 a.m.).

No blinding was applied during sample collection or molecular analyses.

No statistical method was used to predetermine sample size. Sample size was selected based on previous transcriptomic studies and the feasibility of obtaining consistently dissected brain samples. No animals, biological replicates, or sequencing libraries were excluded from the analysis.

5.2.1. Tissue Dissection and Sample Collection

Cockroaches were anesthetized with CO_2 and dissected under Stemi DV4 stereomicroscope (Carl Zeiss, Jena, Germany). Ganglia were dissected in ice-cold cockroach saline (214 mM NaCl, 3.1 mM KCl, 9 mM $CaCl_2$, 50 mM sucrose, 10 mM TES, pH 7.2), prepared according to previously published cockroach saline solutions with minor modification of the buffering agent [105]. The central region of the supraesophageal ganglion containing the central complex and immediately adjacent brain tissue was carefully isolated from the remaining nervous tissue (Figure 8). The subesophageal ganglion (SEG) was not included because the sampling design focused on the supraesophageal brain and its central-complex region; this anatomical restriction does not imply that the SEG is uninvolved in venom-induced locomotor suppression.

The isolated brain regions were immediately transferred into RNase- and DNase-free tubes, snap-frozen in liquid nitrogen, and stored at −80 °C until further processing.

5.2.2. RNA Extraction, Library Preparation and cDNA Library Sequencing

RNA extraction, library preparation and sequencing were performed at Biomarker Technologies (BMK) GmbH (Münster, Germany). Total RNA was extracted from the collected samples and assessed for quantity and integrity using a Qubit 4.0 fluorometer (Thermo Fisher Scientific, Waltham, MA, USA) and automated capillary electrophoresis. mRNA was enriched from total RNA using oligo(dT) magnetic beads, fragmented, and used for the construction of strand-specific (dUTP method) cDNA libraries according to the provider's standard protocol. The libraries were sequenced on an Illumina NovaSeq X Plus platform (Illumina, San Diego, CA, USA) in paired-end mode with a read length of 150 bp, yielding ~10 Gb of raw data per sample.

5.3. Bioinformatic Analysis

5.3.1. RNA-Seq Data Processing and Differential Expression Analysis

Raw sequencing reads were trimmed and filtered using Trimmomatic (version 0.40) [106]. Adapter sequences were removed using the ILLUMINACLIP option with the list of adapters and parameters 2:30:10. The first 10 bases of each read were removed using HEADCROP:10. Low-quality bases were trimmed from the beginning and end of reads using LEADING:3 and TRAILING:3. Additional quality filtering was performed using a sliding window approach (SLIDINGWINDOW:4:20), trimming reads when the average quality score within a four-base window dropped below 20. Reads shorter than 36 bp after trimming were discarded (MINLEN:36). The quality of raw and trimmed reads was assessed using FastQC (version 0.12.1, https://www.bioinformatics.babraham.ac.uk/projects/fastqc/; accessed on 12 November 2026). We checked data for contamination using GenomeFLTR (https://genomefltr.tau.ac.il/; accessed on 12 November 2026). Trimmed reads were then aligned to the reference genome of *Periplaneta americana* (*P. americana* PAMFEO1 priV1; https://www.ncbi.nlm.nih.gov/datasets/genome/GCF_040183065.1/; accessed on 12 November 2026) using HISAT2 (version 2.2.2) with default parameters [107]. Gene annotation from the corresponding

GTF file (https://ftp.ncbi.nlm.nih.gov/genomes/all/GCF/040/183/065/GCF_040183065.1_P.americana_PAMFEO1_priV1/GCF_040183065.1_P.americana_PAMFEO1_priV1_genomic.gtf.gz; accessed on 12 November 2026) was used during downstream analyses. Alignment files were processed using SAMtools (version 1.9) [108]. Gene-level read counts were obtained using featureCounts (version 2.0.6) [109]. Genes with fewer than 10 total reads across all samples were removed prior to further analysis. Differential expression analysis was performed using the R package DESeq2 (version 1.49.3) [110].

5.3.2. Functional Annotation

Functional annotation of predicted proteins was performed using eggNOG-mapper (version 2.1.13) [111], which assigns orthologous groups and functional annotations, including GO terms, based on the eggNOG database. The domain structure of selected proteins was checked using NCBI CD-Search [112] (https://www.ncbi.nlm.nih.gov/Structure/cdd/wrpsb.cgi; accessed on 12 November 2026) against CDD v3.21 [113], and using InterProScan 5 [114] via the InterPro web server (https://www.ebi.ac.uk/interpro/search/sequence/; accessed on 12 November 2026) with InterPro release 110.0 [115]. Both searches were run with default parameters.

5.3.3. Gene Ontology Enrichment Analysis

Gene Ontology (GO) enrichment analysis was conducted using the R package clusterProfiler (v.4.18.2) [116]. Overrepresentation of GO terms was assessed using the hypergeometric test implemented in the enricher function. The analysis was performed separately for the three GO ontologies from Gene Ontology (Biological Process (BP), Molecular Function (MF), Cellular Component (CC)) with the following parameters: *p*-value cutoff: 0.05, q-value cutoff: 0.2, multiple testing correction by the Benjamini–Hochberg method, minimum gene set size: 3, maximum gene set size: 500.

5.3.4. Statistical Analysis and Visualization

Differential expression analysis, GO enrichment analysis, and data visualization were performed in R (version 4.5.0). Principal component analysis (PCA) was performed on variance-stabilized gene-expression data generated using the variance-stabilizing transformation (VST) implemented in DESeq2 (blind = FALSE). The first two principal components (PC1 and PC2) were used to visualize sample clustering, and the proportion of total variance explained by each component was calculated. Group centroids were calculated as the mean PC1 and PC2 coordinates for each experimental group. Differences in multivariate expression profiles between control and stung cockroaches were assessed using permutational multivariate analysis of variance (PERMANOVA), implemented with the adonis2 function in the vegan R package (version 2.7-6). Euclidean distances were calculated from PC1 and PC2 scores, with experimental condition included as the explanatory variable. Normality of ANOVA residuals was assessed before parametric testing. One-way ANOVA was performed separately on PC1 and PC2 scores to test for differences between experimental groups.

5.4. Metabolomics

5.4.1. Experimental Design and Sample Collection

Two experimental groups were established: untreated adult male *P. americana* served as controls (C), whereas the stung group (S) consisted of adult males sampled 24 h after envenomation by the parasitoid wasp *A. compressa*. Only males were used to minimize variation associated with the female reproductive cycle. Each biological replicate consisted of the dissected supraesophageal ganglion from a single individual, with the optic lobes removed. To obtain sufficient tissue for metabolite extraction, metabolomic analysis was

performed using the entire supraoesophageal ganglion, excluding the optic lobes. Five biological replicates ($n = 5$) were obtained for each group. Thus, the metabolomic experiment included 10 individual cockroaches in total. No statistical method was used to predetermine sample size. No animals or metabolomic samples were excluded from the analysis.

To minimize potential circadian effects on metabolite abundance, all dissections were performed at approximately the same time of day (11:00 a.m.). Samples were assigned randomized codes so that group identity was concealed during dissection and subsequent sample processing. The order of sample handling and LC–MS analysis was also randomized to minimize potential operator- and run-order-related biases.

Dissections were performed in ice-cold 150 mM ammonium acetate and completed as rapidly as possible, typically within 2 min. After removal of the surrounding fat tissue, the dissected supraesophageal ganglia were immediately snap-frozen in liquid nitrogen and stored at −80 °C until metabolite extraction.

5.4.2. Metabolite Extraction

Metabolites were extracted as previously described [117], with modifications. Briefly, frozen samples were homogenized using a bead beater, and 500 µL of pre-chilled methanol was added to the resulting tissue powder. Samples were vortexed, supplemented with 100 µL of 0.2% formic acid, mixed, and sonicated. Extraction was then completed using a methanol:chloroform:water mixture.

13C9-15N-phenylalanine and 13C3-lactic acid were added as internal standards before the extraction to a final concentration of 100 µg/mL. The extracts were dried and resuspended in 100 µL of water:acetonitrile (30:70, v/v) and subjected to the liquid-chromatography/mass-spectrometry (LC–MS) analysis.

5.4.3. LC–MS Analysis

LC–MS analysis was performed using an ACQUITY UPLC I-Class Plus system (Waters Corporation, Milford, MA, USA) coupled to a Thermo Scientific Orbitrap Exploris 240 high-resolution mass spectrometer (Thermo Fisher Scientific, Bremen, Germany), following [118] with modifications. Chromatographic separation was achieved using an Atlantis Premier BEH Z-HILIC column (1.7 µm, 2.1 × 100 mm; Waters Corporation, Milford, MA, USA). Mobile phase A consisted of 20 mM ammonium formate, pH 3, in 10% acetonitrile; mobile phase B consisted of 20 mM ammonium formate, pH 3, in 90% acetonitrile. The gradient program was identical to that described previously [118]. The flow rate was 0.3 mL/min, and the injection volume was 1 µL. MS parameters were set according to the manufacturer's recommendations. The data were acquired in full-scan (60–900 Da) mode in positive and negative ionization modes separately.

Blank samples were analyzed to monitor background signals. In addition, three pooled quality-control (QC) samples were analyzed in both full-scan and MS/MS modes to assess analytical performance and obtain secondary fragmentation spectra.

5.4.4. Feature Detection and Metabolite Annotation

Peak detection, extraction, and background filtering were performed using Compound Discoverer v3.3 (Thermo Fisher Scientific, Waltham, MA, USA). Putative metabolite annotation was performed by matching accurate-mass features against the ChemSpider public database and, where MS/MS spectra were available, by comparison with the Thermo Fisher Scientific mzCloud spectral database.

Where reference compounds were available, metabolite identities were further confirmed against an in-house library. Metabolites matched only by accurate mass and/or

public spectral databases were therefore treated as putatively annotated, whereas compounds matched against the in-house library were classified as confirmed.

5.4.5. Statistical Analysis

Downstream statistical analyses were performed using Microsoft Excel for Microsoft 365 (Windows, version 2610, build 20527.20196) and R (version 4.6.2) [119]. PCA was performed using the PCAplotter application (https://scienceinside.shinyapps.io/mvda/; accessed on 12 November 2026).

Differential analysis of metabolic feature abundances between control and stung samples was performed using the limma package (version 3.68.5) [120]. *p*-values were adjusted for multiple testing using the Benjamini–Hochberg false discovery rate (FDR) procedure, and features with FDR < 0.05 were considered statistically significant. Heatmaps were generated using the pheatmap package (version 1.0.13) [121].

5.5. Artificial Intelligence Usage

During preparation of this manuscript, the authors used ChatGPT (GPT-6 Sol, OpenAI) for language editing and assistance in drafting selected passages. Claude AI (Sonnet 4.6, Anthropic) was also used for table editing and preliminary data extraction. Its output was manually checked and edited by the authors. AI was not used to generate or analyze primary experimental data. All scientific interpretations, citations, arguments, and final wording were reviewed and verified by the authors.

Supplementary Materials: The following supporting information can be downloaded at: https://www.mdpi.com/article/10.3390/toxins18110499/s1, Table S1: Differentially expressed genes in the central brain region containing the central complex and adjacent tissue of *Periplaneta americana* 24 h after *Ampulex compressa* envenomation; Table S2: GO Biological Process enrichment analysis of upregulated genes; Table S3: GO Biological Process enrichment analysis of downregulated genes; Table S4: GO Molecular Function enrichment analysis of upregulated genes; Table S5: GO Molecular Function enrichment analysis of downregulated genes; Table S6: GO Cellular Component enrichment analysis of upregulated genes; Table S7: GO Cellular Component enrichment analysis of downregulated genes; Table S8: Processed untargeted metabolomics dataset acquired in positive-ionization mode; Table S9: Processed untargeted metabolomics dataset acquired in negative-ionization mode; Table S10: LC–MS feature-level peak-area data acquired in positive-ionization mode; Table S11: LC–MS feature-level peak-area data acquired in negative-ionization mode.

Author Contributions: Conceptualization, A.M. and F.L.; methodology, A.M. and A.B.; investigation, A.M. and A.B.; formal analysis, A.M., A.L., N.A.P. and A.B.; data curation, A.M., N.A.P. and B.E.; visualization, A.M. and A.L.; writing—original draft preparation, A.M. and A.L.; writing—review and editing, A.M., A.L., N.A.P., A.B., B.E. and F.L.; supervision, F.L.; resources, F.L.; project administration, F.L.; funding acquisition, F.L. All authors have read and agreed to the published version of the manuscript.

Funding: This work was supported by the Kreitman Postdoctoral Fellowship awarded to A.M. and by funds from the Abraham and Bessie Zacks Chair in Neurobiology, held by F.L. at Ben-Gurion University of the Negev. A.L. was supported by a research program of the Zoological Institute RAS, project number FMFG-2026-0002.

Institutional Review Board Statement: Ethical approval was not required under the Israeli Animal Welfare (Experiments on Animals) Law, 5754-1994, which applies to vertebrate animals. This study involved only insects (*Periplaneta americana* and *Ampulex compressa*).

Informed Consent Statement: Not applicable. This study did not involve human participants.

Data Availability Statement: The RNA-sequencing data generated in this study have been deposited in the NCBI Sequence Read Archive (SRA) under BioProject accession PRJNA1541112 (https://www.ncbi.nlm.nih.gov/bioproject/PRJNA1541112; accessed on 12 November 2026). Differential gene-expression results and GO enrichment analyses are provided in Supplementary Tables S1–S7. The complete processed untargeted LC–MS datasets, including metabolite annotations, normalized feature abundances, and statistical analyses, are provided in Supplementary Tables S8 and S9. Feature-level LC–MS data, including integrated peak areas for individual samples, blanks, and quality-control samples, are provided in Supplementary Tables S10 and S11. Additional data supporting the findings of this study are available from the corresponding author upon reasonable request.

Acknowledgments: During the preparation of this manuscript, the authors used ChatGPT (GPT-6 Sol, OpenAI) for language editing and assistance in drafting selected passages. Claude AI (Sonnet 4.6, Anthropic) was also used for table editing and preliminary data extraction. Its output was manually checked and edited by the authors. ChatGPT was not used to generate or analyze primary experimental data. All scientific interpretations, citations, arguments, and final wording were reviewed and verified by the authors, who take full responsibility for the manuscript's content.

Conflicts of Interest: The authors declare no conflicts of interest.

References

1. Adamo, S.A. Modulating the Modulators: Parasites, Neuromodulators and Host Behavioral Change. *Brain Behav. Evol.* **2002**, *60*, 370–377. [CrossRef] [PubMed]
2. Lefèvre, T.; Adamo, S.A.; Biron, D.G.; Missé, D.; Hughes, D.; Thomas, F. Invasion of the Body Snatchers: The Diversity and Evolution of Manipulative Strategies in Host–Parasite Interactions. In *Advances in Parasitology*; Elsevier: Amsterdam, The Netherlands, 2009; Volume 68, pp. 45–83, ISBN 978-0-12-374787-7.
3. Poulin, R. Parasite Manipulation of Host Behavior. In *Advances in the Study of Behavior*; Elsevier: Amsterdam, The Netherlands, 2010; Volume 41, pp. 151–186, ISBN 978-0-12-380892-9.
4. Hughes, D.P.; Libersat, F. Neuroparasitology of Parasite–Insect Associations. *Annu. Rev. Entomol.* **2018**, *63*, 471–487. [CrossRef] [PubMed]
5. Miroliubov, A.; Lianguzova, A.; Libersat, F. Neural Strategies in Parasitic Manipulation. *Trends Parasitol.* **2025**, *41*, 806–819. [CrossRef] [PubMed]
6. Libersat, F.; Haspel, G.; Casagrand, J.; Fouad, K. Localization of the Site of Effect of a Wasp's Venom in the Cockroach Escape Circuitry. *J. Comp. Physiol. A* **1999**, *184*, 333–345. [CrossRef]
7. Haspel, G.; Rosenberg, L.A.; Libersat, F. Direct Injection of Venom by a Predatory Wasp into Cockroach Brain. *J. Neurobiol.* **2003**, *56*, 287–292. [CrossRef] [PubMed]
8. Moore, E.L.; Haspel, G.; Libersat, F.; Adams, M.E. Parasitoid Wasp Sting: A Cocktail of GABA, Taurine, and B-alanine Opens Chloride Channels for Central Synaptic Block and Transient Paralysis of a Cockroach Host. *J. Neurobiol.* **2006**, *66*, 811–820. [CrossRef] [PubMed]
9. Nordio, S.; Kaiser, M.; Adams, M.E.; Libersat, F. Parasitoid Wasp Venom Manipulates Host Innate Behavior via Subtype-Specific Dopamine Receptor Activation. *J. Exp. Biol.* **2022**, *225*, jeb243674. [CrossRef] [PubMed]
10. Rana, A.; Emanuel, S.; Adams, M.E.; Libersat, F. Suppression of Host Nocifensive Behavior by Parasitoid Wasp Venom. *Front. Physiol.* **2022**, *13*, 907041. [CrossRef] [PubMed]
11. Libersat, F. Wasp Uses Venom Cocktail to Manipulate the Behavior of Its Cockroach Prey. *J. Comp. Physiol. A* **2003**, *189*, 497–508. [CrossRef] [PubMed]
12. Gal, R.; Libersat, F. A Parasitoid Wasp Manipulates the Drive for Walking of Its Cockroach Prey. *Curr. Biol.* **2008**, *18*, 877–882. [CrossRef] [PubMed]
13. Gal, R.; Libersat, F. On Predatory Wasps and Zombie Cockroaches: Investigations of Free Will and Spontaneous Behavior in Insects. *Commun. Integr. Biol.* **2010**, *3*, 458–461. [CrossRef] [PubMed]
14. Arvidson, R.; Landa, V.; Frankenberg, S.; Adams, M.E. Life History of the Emerald Jewel Wasp *Ampulex compressa*. *J. Hymenopt. Res.* **2018**, *63*, 1–13. [CrossRef]
15. Arvidson, R.; Kaiser, M.; Lee, S.S.; Urenda, J.-P.; Dail, C.; Mohammed, H.; Nolan, C.; Pan, S.; Stajich, J.E.; Libersat, F.; et al. Parasitoid Jewel Wasp Mounts Multipronged Neurochemical Attack to Hijack a Host Brain. *Mol. Cell. Proteom.* **2019**, *18*, 99–114. [CrossRef] [PubMed]
16. Kaiser, M.; Arvidson, R.; Zarivach, R.; Adams, M.E.; Libersat, F. Molecular Cross-Talk in a Unique Parasitoid Manipulation Strategy. *Insect Biochem. Mol. Biol.* **2019**, *106*, 64–78. [CrossRef] [PubMed]

17. Kaiser, M.; Libersat, F. The Role of the Cerebral Ganglia in the Venom-Induced Behavioral Manipulation of Cockroaches Stung by the Parasitoid Jewel Wasp. *J. Exp. Biol.* **2015**, *218*, 1022–1027. [CrossRef] [PubMed]
18. Rana, A.; Adams, M.E.; Libersat, F. Parasitoid Wasp Venom Re-Programs Host Behavior through Downmodulation of Brain Central Complex Activity and Motor Output. *J. Exp. Biol.* **2023**, *226*, jeb245252. [CrossRef] [PubMed]
19. Banks, C.N.; Adams, M.E. Biogenic Amines in the Nervous System of the Cockroach, *Periplaneta americana* Following Envenomation by the Jewel Wasp, *Ampulex compressa*. *Toxicon* **2012**, *59*, 320–328. [CrossRef] [PubMed]
20. Vickrey, T.L.; Xiao, N.; Venton, B.J. Kinetics of the Dopamine Transporter in *Drosophila* Larva. *ACS Chem. Neurosci.* **2013**, *4*, 832–837. [CrossRef] [PubMed]
21. Muthukumar, A.K.; Stork, T.; Freeman, M.R. Activity-Dependent Regulation of Astrocyte GAT Levels during Synaptogenesis. *Nat. Neurosci.* **2014**, *17*, 1340–1350. [CrossRef] [PubMed]
22. Chen, W.-F.; Maguire, S.; Sowcik, M.; Luo, W.; Koh, K.; Sehgal, A. A Neuron–Glia Interaction Involving GABA Transaminase Contributes to Sleep Loss in Sleepless Mutants. *Mol. Psychiatry* **2015**, *20*, 240–251. [CrossRef] [PubMed]
23. Roeder, T. Tyramine and Octopamine: Ruling Behavior and Metabolism. *Annu. Rev. Entomol.* **2005**, *50*, 447–477. [CrossRef] [PubMed]
24. Saraswati, S.; Fox, L.E.; Soll, D.R.; Wu, C. Tyramine and Octopamine Have Opposite Effects on the Locomotion of *Drosophila* Larvae. *J. Neurobiol.* **2004**, *58*, 425–441. [CrossRef] [PubMed]
25. Schützler, N.; Girwert, C.; Hügli, I.; Mohana, G.; Roignant, J.-Y.; Ryglewski, S.; Duch, C. Tyramine Action on Motoneuron Excitability and Adaptable Tyramine/Octopamine Ratios Adjust *Drosophila* Locomotion to Nutritional State. *Proc. Natl. Acad. Sci. USA* **2019**, *116*, 3805–3810. [CrossRef] [PubMed]
26. Luttrell, L.M.; Gesty-Palmer, D.; Sibley, D.R. Beyond Desensitization: Physiological Relevance of Arrestin-Dependent Signaling. *Pharmacol. Rev.* **2010**, *62*, 305–330. [CrossRef] [PubMed]
27. Zbieralski, K.; Wawrzycka, D. α-Arrestins and Their Functions: From Yeast to Human Health. *Int. J. Mol. Sci.* **2022**, *23*, 4988. [CrossRef] [PubMed]
28. Borbor, S.; Nordio, S.; Libersat, F. Behavioral Recovery Profiling of Cockroaches Stung by the Venomous Wasp *Ampulex compressa*. *J. Exp. Biol.* **2025**, *228*, jeb249768. [CrossRef] [PubMed]
29. Deranieh, R.M.; He, Q.; Caruso, J.A.; Greenberg, M.L. Phosphorylation Regulates Myo-Inositol-3-Phosphate Synthase. *J. Biol. Chem.* **2013**, *288*, 26822–26833. [CrossRef] [PubMed]
30. Van Marrewijk, W.J.A.; Van Den Broek, A.T.M.; Gielbert, M.-L.; Van Der Horst, D.J. Insect Adipokinetic Hormone Stimulates Inositol Phosphate Metabolism: Roles for Both Ins(1,4,5)P3 and Ins(1,3,4,5)P4 in Signal Transduction? *Mol. Cell. Endocrinol.* **1996**, *122*, 141–150. [CrossRef] [PubMed]
31. Poudel, S.; Guo, H.; Smith, D.P. PKC98E Regulates Odorant Responses in *Drosophila melanogaster*. *J. Neurosci.* **2021**, *41*, 3948–3957. [CrossRef] [PubMed]
32. Cheng, Y.L.; Andrew, D.J. Extracellular Mipp1 Activity Confers Migratory Advantage to Epithelial Cells during Collective Migration. *Cell Rep.* **2015**, *13*, 2174–2188. [CrossRef] [PubMed]
33. Sloley, B. Metabolism of Monoamines in Invertebrates: The Relative Importance of Monoamine Oxidase in Different Phyla. *NeuroToxicology* **2004**, *25*, 175–183. [CrossRef] [PubMed]
34. Hiragaki, S.; Suzuki, T.; Mohamed, A.A.M.; Takeda, M. Structures and Functions of Insect Arylalkylamine N-Acetyltransferase (iaaNAT); a Key Enzyme for Physiological and Behavioral Switch in Arthropods. *Front. Physiol.* **2015**, *6*, 113. [CrossRef] [PubMed]
35. Ferguson, L.C.; Green, J.; Surridge, A.; Jiggins, C.D. Evolution of the Insect Yellow Gene Family. *Mol. Biol. Evol.* **2011**, *28*, 257–272. [CrossRef] [PubMed]
36. Zhang, Y.; Li, H.; Du, J.; Zhang, J.; Shen, J.; Cai, W. Three Melanin Pathway Genes, *TH*, *Yellow*, and *aaNAT*, Regulate Pigmentation in the Twin-Spotted Assassin Bug, *Platymeris biguttatus* (Linnaeus). *Int. J. Mol. Sci.* **2019**, *20*, 2728. [CrossRef] [PubMed]
37. Afifi, S.; Wahedi, A.; Paluzzi, J.-P. Functional Insight and Cell-Specific Expression of the Adipokinetic Hormone/Corazonin-Related Peptide in the Human Disease Vector Mosquito, *Aedes aegypti*. *Gen. Comp. Endocrinol.* **2023**, *330*, 114145. [CrossRef] [PubMed]
38. Wahedi, A.; Paluzzi, J.-P. Molecular Identification, Transcript Expression, and Functional Deorphanization of the Adipokinetic Hormone/Corazonin-Related Peptide Receptor in the Disease Vector, *Aedes aegypti*. *Sci. Rep.* **2018**, *8*, 2146. [CrossRef] [PubMed]
39. Verleyen, P.; Chen, X.; Baron, S.; Preumont, A.; Hua, Y.J.; Schoofs, L.; Clynen, E. Cloning of Neuropeptide-like Precursor 1 in the Gray Flesh Fly and Peptide Identification and Expression. *Peptides* **2009**, *30*, 522–530. [CrossRef] [PubMed]
40. Overend, G.; Cabrero, P.; Guo, A.X.; Sebastian, S.; Cundall, M.; Armstrong, H.; Mertens, I.; Schoofs, L.; Dow, J.A.T.; Davies, S.-A. The Receptor Guanylate Cyclase Gyc76C and a Peptide Ligand, NPLP1-VQQ, Modulate the Innate Immune IMD Pathway in Response to Salt Stress. *Peptides* **2012**, *34*, 209–218. [CrossRef] [PubMed]
41. Schoofs, L.; Veelaert, D.; De Loof, A.; Huybrechts, R.; Isaac, E. Immunocytochemical Distribution of Angiotensin I-Converting Enzyme-like Immunoreactivity in the Brain and Testis of Insects. *Brain Res.* **1998**, *785*, 215–227. [CrossRef] [PubMed]

42. Isaac, R.E.; Ekbote, U.; Coates, D.; Shirras, A.D. Insect Angiotensin-converting Enzyme: A Processing Enzyme with Broad Substrate Specificity and a Role in Reproduction. *Ann. N. Y. Acad. Sci.* **1999**, *897*, 342–347. [CrossRef] [PubMed]
43. Liu, Z.; Idris, N.F.B.; Liu, L.; Hou, C.; Yang, C.; Zhan, C.; Liang, S.; Shen, J.; Lu, K.; Hu, H.; et al. BmSV2A and BmSV2B Are Involved in Regulating GABAergic Neuron-Related Gene Expression in the Silkworm, *Bombyx mori*. *Insects* **2025**, *16*, 251. [CrossRef] [PubMed]
44. Aravamudan, B.; Fergestad, T.; Davis, W.S.; Rodesch, C.K.; Broadie, K. *Drosophila* Unc-13 Is Essential for Synaptic Transmission. *Nat. Neurosci.* **1999**, *2*, 965–971. [CrossRef] [PubMed]
45. Piao, C.; Sigrist, S.J. (M)Unc13s in Active Zone Diversity: A *Drosophila* Perspective. *Front. Synaptic Neurosci.* **2022**, *13*, 798204. [CrossRef] [PubMed]
46. Linial, M.; Miller, K.; Scheller, R.H. VAT 1: An Abundant Membrane Protein from *Torpedo* Cholinergic Synaptic Vesicles. *Neuron* **1989**, *2*, 1265–1273. [CrossRef] [PubMed]
47. Young, J.M.; Armstrong, J.D. Building the Central Complex in *Drosophila*: The Generation and Development of Distinct Neural Subsets. *J. Comp. Neurol.* **2010**, *518*, 1525–1541. [CrossRef] [PubMed]
48. Omoto, J.J.; Nguyen, B.-C.M.; Kandimalla, P.; Lovick, J.K.; Donlea, J.M.; Hartenstein, V. Neuronal Constituents and Putative Interactions Within the *Drosophila* Ellipsoid Body Neuropil. *Front. Neural Circuits* **2018**, *12*, 103. [CrossRef] [PubMed]
49. Hoerndli, F.J.; Walser, M.; Fröhli Hoier, E.; De Quervain, D.; Papassotiropoulos, A.; Hajnal, A. A Conserved Function of *C. elegans* CASY-1 Calsyntenin in Associative Learning. *PLoS ONE* **2009**, *4*, e4880. [CrossRef] [PubMed]
50. Mori, K.; Koebis, M.; Nakao, K.; Kobayashi, S.; Kiyama, Y.; Watanabe, M.; Manabe, T.; Iino, Y.; Aiba, A. Loss of Calsyntenin Paralogs Disrupts Interneuron Stability and Mouse Behavior. *Mol. Brain* **2022**, *15*, 23. [CrossRef] [PubMed]
51. Pézier, A.P.; Jezzini, S.H.; Bacon, J.P.; Blagburn, J.M. Shaking B Mediates Synaptic Coupling between Auditory Sensory Neurons and the Giant Fiber of *Drosophila melanogaster*. *PLoS ONE* **2016**, *11*, e0152211. [CrossRef] [PubMed]
52. Hürkey, S.; Niemeyer, N.; Schleimer, J.-H.; Ryglewski, S.; Schreiber, S.; Duch, C. Gap Junctions Desynchronize a Neural Circuit to Stabilize Insect Flight. *Nature* **2023**, *618*, 118–125. [CrossRef] [PubMed]
53. Raccuglia, D.; Suárez-Grimalt, R.; Krumm, L.; Ender, A.; Brodersen, C.B.; Jagannathan, S.R.; Freire Krück, M.; Pampaloni, N.P.; Rauch, C.; Winter, Y.; et al. Network Synchrony Creates Neural Filters Promoting Quiescence in *Drosophila*. *Nature* **2025**, *646*, 667–675. [CrossRef] [PubMed]
54. Ballard, S.L.; Miller, D.L.; Ganetzky, B. Retrograde Neurotrophin Signaling through Tollo Regulates Synaptic Growth in *Drosophila*. *J. Cell Biol.* **2014**, *204*, 1157–1172. [CrossRef] [PubMed]
55. Fujita, N.; Nagata, Y.; Nishiuchi, T.; Sato, M.; Iwami, M.; Kiya, T. Visualization of Neural Activity in Insect Brains Using a Conserved Immediate Early Gene, *Hr38*. *Curr. Biol.* **2013**, *23*, 2063–2070. [CrossRef] [PubMed]
56. Sommerlandt, F.M.J.; Brockmann, A.; Rössler, W.; Spaethe, J. Immediate Early Genes in Social Insects: A Tool to Identify Brain Regions Involved in Complex Behaviors and Molecular Processes Underlying Neuroplasticity. *Cell. Mol. Life Sci.* **2019**, *76*, 637–651. [CrossRef] [PubMed]
57. Horne, M.; Krebushevski, K.; Wells, A.; Tunio, N.; Jarvis, C.; Francisco, G.; Geiss, J.; Recknagel, A.; Deitcher, D.L. Julius Seizure, a *Drosophila* Mutant, Defines a Neuronal Population Underlying Epileptogenesis. *Genetics* **2017**, *205*, 1261–1269. [CrossRef] [PubMed]
58. Jetti, S.K.; Crane, A.B.; Akbergenova, Y.; Aponte-Santiago, N.A.; Cunningham, K.L.; Whittaker, C.A.; Littleton, J.T. Molecular Logic of Synaptic Diversity between *Drosophila* Tonic and Phasic Motoneurons. *Neuron* **2023**, *111*, 3554–3569.e7. [CrossRef] [PubMed]
59. Tiebe, M.; Lutz, M.; De La Garza, A.; Buechling, T.; Boutros, M.; Teleman, A.A. *REPTOR* and REPTOR-BP Regulate Organismal Metabolism and Transcription Downstream of TORC1. *Dev. Cell* **2015**, *33*, 272–284. [CrossRef] [PubMed]
60. Limmer, S.; Weiler, A.; Volkenhoff, A.; Babatz, F.; Klämbt, C. The *Drosophila* Blood-Brain Barrier: Development and Function of a Glial Endothelium. *Front. Neurosci.* **2014**, *8*, 365. [CrossRef] [PubMed]
61. Laughlin, S.B.; de Ruyter van Steveninck, R.R.; Anderson, J.C. The Metabolic Cost of Neural Information. *Nat. Neurosci.* **1998**, *1*, 36–41. [CrossRef] [PubMed]
62. Zhang, H.; Tang, B.; Lin, Y.; Chen, Z.; Zhang, X.; Ji, T.; Zhang, X.; Hou, Y. Identification of Three Prophenoloxidase-activating Factors (PPAFs) from an Invasive Beetle *Octodonta nipae* Maulik (Coleoptera: Chrysomelidae) and Their Roles in the Prophenoloxidase Activation. *Arch. Insect Biochem. Physiol.* **2017**, *96*, e21425. [CrossRef] [PubMed]
63. Zhang, X.; Zhang, S.; Kuang, J.; Sellens, K.A.; Morejon, B.; Saab, S.A.; Li, M.; Metto, E.C.; An, C.; Culbertson, C.T.; et al. CLIPB4 Is a Central Node in the Protease Network That Regulates Humoral Immunity in *Anopheles gambiae* Mosquitoes. *J. Innate Immun.* **2023**, *15*, 680–696. [CrossRef] [PubMed]
64. Piao, S.; Song, Y.; Kim, J.H.; Park, S.Y.; Park, J.W.; Lee, B.L.; Oh, B.; Ha, N. Crystal Structure of a Clip-domain Serine Protease and Functional Roles of the Clip Domains. *EMBO J.* **2005**, *24*, 4404–4414. [CrossRef] [PubMed]
65. Jin, Q.; Wang, Y.; Yin, H.; Jiang, H. Two Clip-Domain Serine Protease Homologs, cSPH35 and cSPH242, Act as a Cofactor for Prophenoloxidase-1 Activation in *Drosophila melanogaster*. *Front. Immunol.* **2023**, *14*, 1244792. [CrossRef] [PubMed]

66. Nam, H.; Jang, I.; You, H.; Lee, K.; Lee, W. Genetic Evidence of a Redox-dependent Systemic Wound Response via Hayan Protease-Phenoloxidase System in *Drosophila*. *EMBO J.* **2012**, *31*, 1253–1265. [CrossRef] [PubMed]
67. Chen, C.; Rowley, A.F.; Newton, R.P.; Ratcliffe, N.A. Identification, Purification and Properties of a β-1,3-Glucan-Specific Lectin from the Serum of the Cockroach, *Blaberus discoidalis* Which Is Implicated in Immune Defence Reactions. *Comp. Biochem. Physiol. B Biochem. Mol. Biol.* **1999**, *122*, 309–319. [CrossRef] [PubMed]
68. Bischoff, V.; Vignal, C.; Boneca, I.G.; Michel, T.; Hoffmann, J.A.; Royet, J. Function of the *Drosophila* Pattern-Recognition Receptor PGRP-SD in the Detection of Gram-Positive Bacteria. *Nat. Immunol.* **2004**, *5*, 1175–1180. [CrossRef] [PubMed]
69. Bischoff, V.; Vignal, C.; Duvic, B.; Boneca, I.G.; Hoffmann, J.A.; Royet, J. Downregulation of the *Drosophila* Immune Response by Peptidoglycan-Recognition Proteins SC1 and SC2. *PLoS Pathog.* **2006**, *2*, e14. [CrossRef] [PubMed]
70. Chapelle, M.; Girard, P.-A.; Cousserans, F.; Volkoff, N.-A.; Duvic, B. Lysozymes and Lysozyme-like Proteins from the Fall Armyworm, *Spodoptera frugiperda*. *Mol. Immunol.* **2009**, *47*, 261–269. [CrossRef] [PubMed]
71. Liu, Z.; Yuan, K.; Zhang, R.; Ren, X.; Liu, X.; Zhao, S.; Wang, D. Cloning and Purification of the First Termicin-like Peptide from the Cockroach *Eupolyphaga sinensis*. *J. Venom. Anim. Toxins Incl. Trop. Dis.* **2016**, *22*, 5. [CrossRef] [PubMed]
72. Gao, F.; Gu, Q.; Pan, J.; Wang, Z.; Yin, C.; Li, F.; Song, Q.; Strand, M.R.; Chen, X.; Shi, M. *Cotesia vestalis* Teratocytes Express a Diversity of Genes and Exhibit Novel Immune Functions in Parasitism. *Sci. Rep.* **2016**, *6*, 26967. [CrossRef] [PubMed]
73. Dos Santos Cabrera, M.P.; Rangel, M.; Ruggiero Neto, J.; Konno, K. Chemical and Biological Characteristics of Antimicrobial α-Helical Peptides Found in Solitary Wasp Venoms and Their Interactions with Model Membranes. *Toxins* **2019**, *11*, 559. [CrossRef] [PubMed]
74. Zhou, L.; Wang, R.; Lin, Z.; Shi, S.; Chen, C.; Jiang, H.; Zou, Z.; Lu, Z. Two Venom Serpins from the Parasitoid Wasp *Microplitis mediator* Inhibit the Host Prophenoloxidase Activation and Antimicrobial Peptide Synthesis. *Insect Biochem. Mol. Biol.* **2023**, *152*, 103895. [CrossRef] [PubMed]
75. Sawicki, R.; Singh, S.P.; Mondal, A.K.; Beneš, H.; Zimniak, P. Cloning, Expression and Biochemical Characterization of One Epsilon-Class (GST-3) and Ten Delta-Class (GST-1) Glutathione S-Transferases from *Drosophila melanogaster*, and Identification of Additional Nine Members of the Epsilon Class. *Biochem. J.* **2003**, *370*, 661–669. [CrossRef] [PubMed]
76. Udomsinprasert, R.; Pongjaroenkit, S.; Wongsantichon, J.; Oakley, A.J.; Prapanthadara, L.; Wilce, M.C.J.; Ketterman, A.J. Identification, Characterization and Structure of a New Delta Class Glutathione Transferase Isoenzyme. *Biochem. J.* **2005**, *388*, 763–771. [CrossRef] [PubMed]
77. Hassan, F.; Singh, K.P.; Ali, V.; Behera, S.; Shivam, P.; Das, P.; Dinesh, D.S. Detection and Functional Characterization of Sigma Class GST in *Phlebotomus argentipes* and Its Role in Stress Tolerance and DDT Resistance. *Sci. Rep.* **2019**, *9*, 19636. [CrossRef] [PubMed]
78. Song, X.; Zhong, Q.; Ji, Y.; Zhang, Y.; Tang, J.; Feng, F.; Bi, J.; Xie, J.; Li, B. Characterization of a Sigma Class GST (GSTS6) Required for Cellular Detoxification and Embryogenesis in *Tribolium castaneum*. *Insect Sci.* **2022**, *29*, 215–229. [CrossRef] [PubMed]
79. Zhu, F.; Parthasarathy, R.; Bai, H.; Woithe, K.; Kaussmann, M.; Nauen, R.; Harrison, D.A.; Palli, S.R. A Brain-Specific Cytochrome P450 Responsible for the Majority of Deltamethrin Resistance in the QTC279 Strain of *Tribolium castaneum*. *Proc. Natl. Acad. Sci. USA* **2010**, *107*, 8557–8562. [CrossRef] [PubMed]
80. Maibèche-Coisne, M.; Monti-Dedieu, L.; Aragon, S.; Dauphin-Villemant, C. A New Cytochrome P450 from *Drosophila melanogaster*, CYP4G15, Expressed in the Nervous System. *Biochem. Biophys. Res. Commun.* **2000**, *273*, 1132–1137. [CrossRef] [PubMed]
81. Kim, B.Y.; Lee, K.S.; Choo, Y.M.; Kim, I.; Je, Y.H.; Woo, S.D.; Lee, S.M.; Park, H.C.; Sohn, H.D.; Jin, B.R. Insect Transferrin Functions as an Antioxidant Protein in a Beetle Larva. *Comp. Biochem. Physiol. B Biochem. Mol. Biol.* **2008**, *150*, 161–169. [CrossRef] [PubMed]
82. Geiser, D.L.; Winzerling, J.J. Insect Transferrins: Multifunctional Proteins. *Biochim. Biophys. Acta BBA—Gen. Subj.* **2012**, *1820*, 437–451. [CrossRef] [PubMed]
83. Weber, J.J.; Kanost, M.R.; Gorman, M.J. Iron Binding and Release Properties of Transferrin-1 from *Drosophila melanogaster* and *Manduca sexta*: Implications for Insect Iron Homeostasis. *Insect Biochem. Mol. Biol.* **2020**, *125*, 103438. [CrossRef] [PubMed]
84. Najera, D.G.; Dittmer, N.T.; Weber, J.J.; Kanost, M.R.; Gorman, M.J. Phylogenetic and Sequence Analyses of Insect Transferrins Suggest That Only Transferrin 1 Has a Role in Iron Homeostasis. *Insect Sci.* **2021**, *28*, 495–508. [CrossRef] [PubMed]
85. Meyer, S.; Schmidt, I.; Klämbt, C. Glia ECM Interactions Are Required to Shape the *Drosophila* Nervous System. *Mech. Dev.* **2014**, *133*, 105–116. [CrossRef] [PubMed]
86. Deák, F.; Wagener, R.; Kiss, I.; Paulsson, M. The Matrilins: A Novel Family of Oligomeric Extracellular Matrix Proteins. *Matrix Biol.* **1999**, *18*, 55–64. [CrossRef] [PubMed]
87. Klatt, A.R.; Becker, A.-K.A.; Neacsu, C.D.; Paulsson, M.; Wagener, R. The Matrilins: Modulators of Extracellular Matrix Assembly. *Int. J. Biochem. Cell Biol.* **2011**, *43*, 320–330. [CrossRef] [PubMed]
88. Malin, D.; Sonnenberg-Riethmacher, E.; Guseva, D.; Wagener, R.; Aszódi, A.; Irintchev, A.; Riethmacher, D. The Extracellular-Matrix Protein Matrilin 2 Participates in Peripheral Nerve Regeneration. *J. Cell Sci.* **2009**, *122*, 995–1004. [CrossRef] [PubMed]

89. Korpos, É.; Deák, F.; Kiss, I. Matrilin-2, an Extracellular Adaptor Protein, Is Needed for the Regeneration of Muscle, Nerve and Other Tissues. *Neural Regen. Res.* **2015**, *10*, 866. [CrossRef] [PubMed]
90. Yun, S.-J.; Kim, M.-O.; Kim, S.O.; Park, J.; Kwon, Y.K.; Kim, I.-S.; Lee, E.H. Induction of TGF-β-Inducible Gene-H3 (Big-H3) by TGF-B1 in Astrocytes: Implications for Astrocyte Response to Brain Injury. *Mol. Brain Res.* **2002**, *107*, 57–64. [CrossRef] [PubMed]
91. Luo, J. TGF-β as a Key Modulator of Astrocyte Reactivity: Disease Relevance and Therapeutic Implications. *Biomedicines* **2022**, *10*, 1206. [CrossRef] [PubMed]
92. Troyanovsky, B.; Levchenko, T.; Månsson, G.; Matvijenko, O.; Holmgren, L. Angiomotin: An Angiostatin Binding Protein That Regulates Endothelial Cell Migration and Tube Formation. *J. Cell Biol.* **2001**, *152*, 1247–1254. [CrossRef] [PubMed]
93. Wang, W.; Huang, J.; Chen, J. Angiomotin-like Proteins Associate with and Negatively Regulate YAP1. *J. Biol. Chem.* **2011**, *286*, 4364–4370. [CrossRef] [PubMed]
94. Kolpakova, E.; Rusten, T.E.; Olsnes, S. Characterization and Tissue Expression of Acidic Fibroblast Growth Factor Binding Protein Homologue in *Drosophila melanogaster*. *Gene* **2003**, *310*, 185–191. [CrossRef] [PubMed]
95. Beermann, A.; Schröder, R. Sites of Fgf Signalling and Perception during Embryogenesis of the Beetle *Tribolium castaneum*. *Dev. Genes Evol.* **2008**, *218*, 153–167. [CrossRef] [PubMed]
96. Oulion, S.; Bertrand, S.; Escriva, H. Evolution of the FGF Gene Family. *Int. J. Evol. Biol.* **2012**, *2012*, 298147. [CrossRef] [PubMed]
97. Li, J.; Wang, Q.; Cai, H.; He, Z.; Wang, H.; Chen, J.; Zheng, Z.; Yin, J.; Liao, Z.; Xu, H.; et al. FGF 1 Improves Functional Recovery through Inducing PRDX 1 to Regulate Autophagy and anti-ROS after Spinal Cord Injury. *J. Cell. Mol. Med.* **2018**, *22*, 2727–2738. [CrossRef] [PubMed]
98. Hunt, D.; Raivich, G.; Anderson, P.N. Activating Transcription Factor 3 and the Nervous System. *Front. Mol. Neurosci.* **2012**, *5*, 7. [CrossRef] [PubMed]
99. Katz, H.R.; Arcese, A.A.; Bloom, O.; Morgan, J.R. Activating Transcription Factor 3 (ATF3) Is a Highly Conserved Pro-Regenerative Transcription Factor in the Vertebrate Nervous System. *Front. Cell Dev. Biol.* **2022**, *10*, 824036. [CrossRef] [PubMed]
100. Banfi, D.; Bianchi, T.; Mastore, M.; Brivio, M.F. The Role of Heat Shock Proteins in Insect Stress Response, Immunity, and Climate Adaptation. *Insects* **2025**, *16*, 741. [CrossRef] [PubMed]
101. Walther, D.; Strassburg, K.; Durek, P.; Kopka, J. Metabolic Pathway Relationships Revealed by an Integrative Analysis of the Transcriptional and Metabolic Temperature Stress-Response Dynamics in Yeast. *OMICS J. Integr. Biol.* **2010**, *14*, 261–274. [CrossRef] [PubMed]
102. Takahashi, H.; Morioka, R.; Ito, R.; Oshima, T.; Altaf-Ul-Amin, M.; Ogasawara, N.; Kanaya, S. Dynamics of Time-Lagged Gene-to-Metabolite Networks of *Escherichia coli* Elucidated by Integrative Omics Approach. *OMICS J. Integr. Biol.* **2011**, *15*, 15–23. [CrossRef] [PubMed]
103. Fernie, A.R.; Stitt, M. On the Discordance of Metabolomics with Proteomics and Transcriptomics: Coping with Increasing Complexity in Logic, Chemistry, and Network Interactions Scientific Correspondence. *Plant Physiol.* **2012**, *158*, 1139–1145. [CrossRef] [PubMed]
104. Buescher, J.M.; Driggers, E.M. Integration of Omics: More than the Sum of Its Parts. *Cancer Metab.* **2016**, *4*, 4. [CrossRef] [PubMed]
105. Weisel-Eichler, A.; Libersat, F. Are Monoaminergic Systems Involved in the Lethargy Induced by a Parasitoid Wasp in the Cockroach Prey? *J. Comp. Physiol. A* **2002**, *188*, 315–324. [CrossRef] [PubMed]
106. Bolger, A.M.; Lohse, M.; Usadel, B. Trimmomatic: A Flexible Trimmer for Illumina Sequence Data. *Bioinformatics* **2014**, *30*, 2114–2120. [CrossRef] [PubMed]
107. Kim, D.; Paggi, J.M.; Park, C.; Bennett, C.; Salzberg, S.L. Graph-Based Genome Alignment and Genotyping with HISAT2 and HISAT-Genotype. *Nat. Biotechnol.* **2019**, *37*, 907–915. [CrossRef] [PubMed]
108. Li, H.; Handsaker, B.; Wysoker, A.; Fennell, T.; Ruan, J.; Homer, N.; Marth, G.; Abecasis, G.; Durbin, R.; 1000 Genome Project Data Processing Subgroup. The Sequence Alignment/Map Format and SAMtools. *Bioinformatics* **2009**, *25*, 2078–2079. [CrossRef] [PubMed]
109. Liao, Y.; Smyth, G.K.; Shi, W. featureCounts: An Efficient General Purpose Program for Assigning Sequence Reads to Genomic Features. *Bioinformatics* **2014**, *30*, 923–930. [CrossRef] [PubMed]
110. Love, M.I.; Huber, W.; Anders, S. Moderated Estimation of Fold Change and Dispersion for RNA-Seq Data with DESeq2. *Genome Biol.* **2014**, *15*, 550. [CrossRef] [PubMed]
111. Cantalapiedra, C.P.; Hernández-Plaza, A.; Letunic, I.; Bork, P.; Huerta-Cepas, J. eggNOG-Mapper v2: Functional Annotation, Orthology Assignments, and Domain Prediction at the Metagenomic Scale. *Mol. Biol. Evol.* **2021**, *38*, 5825–5829. [CrossRef] [PubMed]
112. Marchler-Bauer, A.; Bryant, S.H. CD-Search: Protein Domain Annotations on the Fly. *Nucleic Acids Res.* **2004**, *32*, W327–W331. [CrossRef] [PubMed]
113. Wang, J.; Chitsaz, F.; Derbyshire, M.K.; Gonzales, N.R.; Gwadz, M.; Lu, S.; Marchler, G.H.; Song, J.S.; Thanki, N.; Yamashita, R.A.; et al. The Conserved Domain Database in 2023. *Nucleic Acids Res.* **2023**, *51*, D384–D388. [CrossRef] [PubMed]

114. Jones, P.; Binns, D.; Chang, H.-Y.; Fraser, M.; Li, W.; McAnulla, C.; McWilliam, H.; Maslen, J.; Mitchell, A.; Nuka, G.; et al. InterProScan 5: Genome-Scale Protein Function Classification. *Bioinformatics* **2014**, *30*, 1236–1240. [CrossRef] [PubMed]
115. Blum, M.; Hobbs, E.; Florentino, L.; Bateman, A. InterProScan 6: A Modern Large-Scale Protein Function Annotation Pipeline. *Bioinforma. Adv.* **2026**, *6*, vbag141. [CrossRef] [PubMed]
116. Wu, T.; Hu, E.; Xu, S.; Chen, M.; Guo, P.; Dai, Z.; Feng, T.; Zhou, L.; Tang, W.; Zhan, L.; et al. clusterProfiler 4.0: A Universal Enrichment Tool for Interpreting Omics Data. *Innovation* **2021**, *2*, 100141. [CrossRef] [PubMed]
117. Batushansky, A.; Lopes, E.B.P.; Zhu, S.; Humphries, K.M.; Griffin, T.M. GC–MS Method for Metabolic Profiling of Mouse Femoral Head Articular Cartilage Reveals Distinct Effects of Tissue Culture and Development. *Osteoarthr. Cartil.* **2019**, *27*, 1361–1371. [CrossRef] [PubMed]
118. Lemcoff, T.; Alus, L.; Batushansky, A.; Fishman, Y.; Theodor, N.; Shavit, K.; Hyitner, L.; Kelber, A.; Haataja, J.S.; Oron, D.; et al. Damselflies Overcome Color Saturation Barriers of Photonic Glasses via Pigment Loading and Refractive Index Modulation. *Proc. Natl. Acad. Sci. USA* **2026**, *123*, e2527433123. [CrossRef] [PubMed]
119. R Core Team. *R: A Language and Environment for Statistical Computing*; R Foundation for Statistical Computing: Vienna, Austria, 2021.
120. Ritchie, M.E.; Phipson, B.; Wu, D.; Hu, Y.; Law, C.W.; Shi, W.; Smyth, G.K. Limma Powers Differential Expression Analyses for RNA-Sequencing and Microarray Studies. *Nucleic Acids Res.* **2015**, *43*, e47. [CrossRef] [PubMed]
121. Kolde, R. *Pheatmap: Pretty Heatmaps*; CRAN: Vienna, Austria, 2019. Available online: https://cran.r-project.org/package=pheatmap (accessed on 12 November 2026).

Disclaimer/Publisher's Note: The statements, opinions and data contained in all publications are solely those of the individual author(s) and contributor(s) and not of MDPI and/or the editor(s). MDPI and/or the editor(s) disclaim responsibility for any injury to people or property resulting from any ideas, methods, instructions or products referred to in the content.